AD-A116 125 ARTEC ASSOCIATES INC HAYWARD CA F/G 20/9
DENSE, NONIDEAL PLASMA RESEARCH.(U)
APR 81 D W BAUM, S P GILL, W L SHIMMIN N00014-78-C-0354
UNCLASSIFIED AR-130 NL

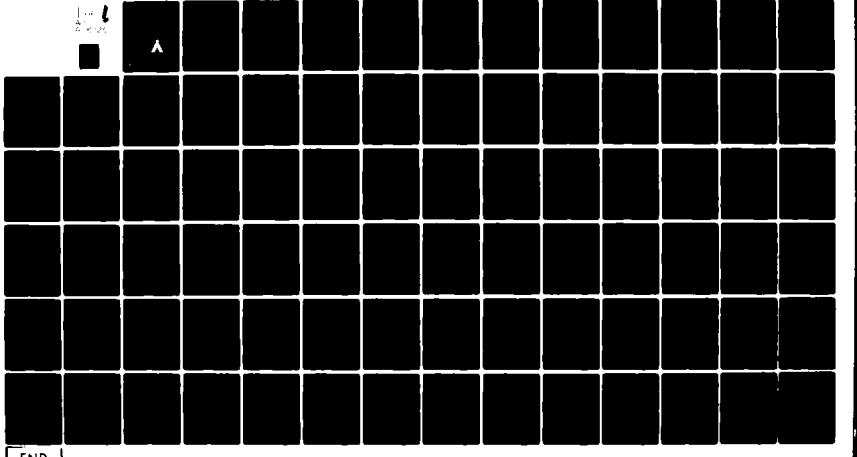

END
DATE FILED
DTIC

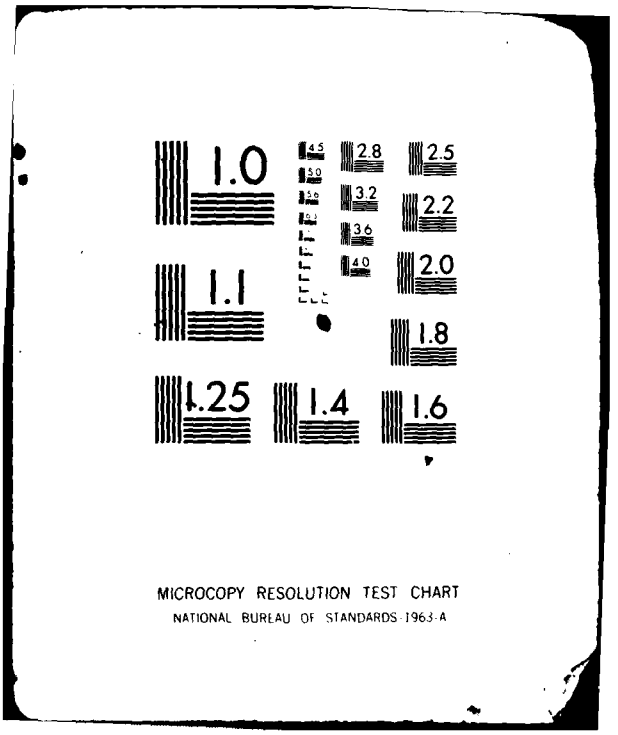
1.0
1.1
1.25
1.4
1.6
1.8
2.0
2.2
2.5
2.8
3.2
3.6
4.0
4.5
5.0
MICROCOPY RESOLUTION TEST CHART
NATIONAL BUREAU OF STANDARDS-1963-A

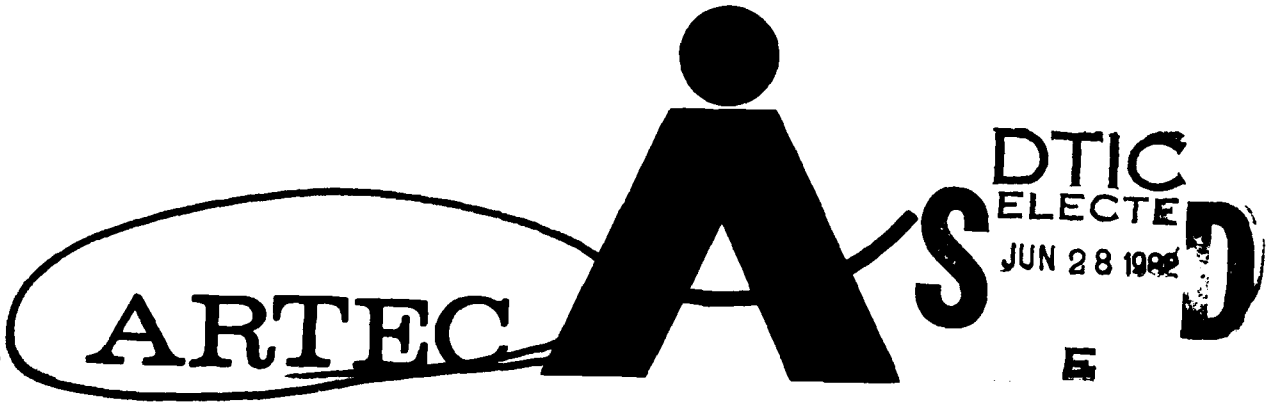

(1)

Dense Nonideal Plasma Research

Annual Report 130

30 April 1981
Final Report for Period 15 April 1979 to
14 March 1981

Sponsored by: Office of Naval Research
Department of the Navy
800 North Quincy Street
Arlington, Virginia 22217
Requisition Authority No.
NR099-418/8-27-80 (473)
Contract No. N00014-78-C-0354

Prepared by: Dennis W. Baum, Stephen P. Gill,
W. Lee Shimmin and John D. Watson

Artec Associates Incorporated
26046 Eden Landing Road
Hayward, California 94545
Telephone: 415/785-8080

UNCLASSIFIED

SECURITY CLASSIFICATION OF THIS PAGE (When Data Entered)

REPORT DOCUMENTATION PAGE	READ INSTRUCTIONS BEFORE COMPLETING FORM
1. REPORT NUMBER: AR-130	2. GOVT ACCESSION NO.: AD-A116 125
3. RECIPIENT'S CATALOG NUMBER:	
4. TITLE (and Subtitle): Dense, Nonideal Plasma Research	5. TYPE OF REPORT & PERIOD COVERED: Annual Report 16 Apr 79 to 14 Mar 81
	6. PERFORMING ORG. REPORT NUMBER:
7. AUTHOR(s): Dennis W. Baum, Stephen P. Gill, W. Lee Shimmin and John D. Watson	8. CONTRACT OR GRANT NUMBER(s): N00014-78-C-0354
9. PERFORMING ORGANIZATION NAME AND ADDRESS: Artec Associates Incorporated 26046 Eden Landing Road Hayward, California 94545	10. PROGRAM ELEMENT, PROJECT, TASK AREA & WORK UNIT NUMBERS: 122401
11. CONTROLLING OFFICE NAME AND ADDRESS: Office of Naval Research, Dept. of Navy 800 North Quincy Street Arlington, Virginia 22217	12. REPORT DATE: 30 April 1981
	13. NUMBER OF PAGES: 80
14. MONITORING AGENCY NAME & ADDRESS(if different from Controlling Office)	15. SECURITY CLASS. (of this report): Unclassified
	15a. DECLASSIFICATION/DOWNGRADING SCHEDULE:
16. DISTRIBUTION STATEMENT (of this Report): Approved for Public Release; Distribution Unlimited	
17. DISTRIBUTION STATEMENT (of the abstract entered in Block 20, if different from Report):	
18. SUPPLEMENTARY NOTES:	
19. KEY WORDS (Continue on reverse side if necessary and identify by block number): Dense Nonideal Plasma; Magnetohydrodynamics; Argon Electrical Conductivity; Pulsed MHD Power; Plasma Source; Prime Power Source	

20. ABSTRACT (Continue on reverse side if necessary and identify by block number)

Experimental and theoretical research on argon, xenon and air dense nonideal plasmas is reported. The study is focussed on the factors controlling specific energy, electrical conductivity and flow variables of a plasma pulse from an energetic explosively driven plasma source. Measurements and analyses of the plasma pulse passing through a magnetic field are reported. An average electrical power density output of 2.4 TW/m^3-T^2 was measured for a 2.5 MJ plasma pulse.

DD FORM 1 JAN 73 1473 EDITION OF 1 NOV 65 IS OBSOLETE

Unclassified

SECURITY CLASSIFICATION OF THIS PAGE (When Data Entered)

TITLE: (U) NON-IDEAL PLASMA
AGENCY ACCESSION NO: DN875392
DATE OF SUMMARY: 03 DEC 80
PRIMARY PROGRAM ELEMENT: 61153N
PRIMARY PROJECT NUMBER: RR02401
- PRIMARY PROJECT AGENCY AND PROGRAM: RR02401
PRIMARY TASK AREA: RR0240101
WORK UNIT NUMBER: NR-099-418
CONTRACT/GRANT NUMBER: N00014-78-C-0354
DOD ORGANIZATION: OFFICE OF NAVAL RESEARCH (473)
DOD ORG. ADDRESS: ARLINGTON, VA 22217
RESPONSIBLE INDIVIDUAL: SATKOWSKI, J A 473
RESPONSIBLE INDIVIDUAL PHONE: 202-696-4406
DOD ORGANIZATION LOCATION CODE: 5110
DOD ORGANIZATION SORT CODE: 35832
DOD ORGANIZATION CODE: 265250
PERFORMING ORGANIZATION: ARTEC ASSOCIATES, INC.
PERFORMING ORG. ADDRESS: HAYWARD, CA 94545
PRINCIPAL INVESTIGATOR: FLAGG, R F
PRINCIPAL INVESTIGATOR PHONE: 415-875-8080
PERFORMING ORGANIZATION LOCATION CODE: 0609
- PERF. ORGANIZATION TYPE CODE: 4
- PERFORMING ORG. SORT CODE: 05500
- PERFORMING ORGANIZATION CODE: 408296
- TECHNICAL OBJECTIVE: (U) THE OBJECTIVE OF THIS WOEK IS TO INVESTIGATE EFFICIENT MEANS OF SHOCK HEATING HEAVY RARE GASES DIRECTLY FROM EXPLOSIVES IN ORDER TO PRODUCE A HOT, DENSE, NON-IDEAL PLASMA WITH HIGH ELECTRICAL CONDUCTIVITY SUITABLE FOR USE IN A PULSED ELECTRICAL POWER MHD DEVICE FOR NAVAL WEAPON APPLICATIONS
- KEYWORDS: (U) HIGH TEMPERATURE PLASMA ;(U) MHD ELECTRICAL PULSED POWER ;(U) NAVAL WEAPONS ;(U) EXPLOSIVE DRIVEN ASSEMBLIES ;
- DESCRIPTORS: (U) ARGON ;(U) CHEMICAL REACTIONS;(U) ELECTRON DENSITY ;(U) ELECTRICAL CONDUCTIVITY ;(U) ENERGY;(U) ENERGY TRANSFER ;(U) HIGH TEMPERATURE ;(U) ENERGY CONVERSION ;(U) PLASMAS(PHYSICS) ; (U) THERMAL RADIATION ;(U) SHOCK WAVES ;(U) WEAPONS ;(U) WORK ; (U) NAVAL EQUIPMENT ;
**

<<ENTER NEXT COMMAND>>

Table of Contents

List of Figures

List of Figures
(Continued)

List of Figures
(Continued)

List of Tables

Acknowledgements

The work presented in this report was sponsored by the Office of Naval Research under Contract N00014-78-C-0354 in support of the ONR Power Program under the direction of Mr. J. A. Satkowski. His encouragement and direction are gratefully acknowledged by the authors. We would also like to express our thanks to Dr. E. T. Florance of the ONR Pasadena Office for serving as Scientific Officer for the program.

The work was carried out by Artec Associates Incorporated in Hayward, California. Dr. Dennis W. Baum served as principal investigator. Dr. Stephen P. Gill provided continuing support of the experimental, computational and theoretical aspects of the program. The experimental work reported herein was directed by Dr. R. F. Flagg. Mr. J. D. Watson carried out the computational work. Dr. Flagg, Mr. Watson and Mr. W. Lee Shimmin participated in the data analysis. Mr. Thomas Bratton and Mr. Peter Vance were responsible for fabricating the experiments and assisted in the tests.

We are especially grateful to the Lawrence Livermore National Laboratory for providing experimental services and support for our tests at Site 300. We also wish to thank Dr. Forrest Rogers and his co-workers at LLNL for providing the information on the argon equation-of-state and argon conductivities.

1.0 Introduction

This annual report summarizes research for the period 15 April 1979 to 14 March 1981 on the measurement and analysis of dense non-ideal plasmas generated by a compact, explosively driven device. In previous programs dating back to 1976, Artec Associates has pursued a program of basic research in pulsed plasma MHD (References 1, 2 and 3). As a result, our knowledge of the properties of dense non-ideal plasmas has been greatly expanded. We have generated plasma states intermediate to those achieved by chemical and nuclear explosive means; we have experimentally measured plasma electrical conductivity and flow velocity histories; and we have helped define the theoretical framework for predicting conductivities in the dense non-ideal regime.

The results of the present work have extended our knowledge and now form the underlying theoretical and experimental basis for pulsed plasma MHD as a compact primary power source capable of megajoule electrical pulses at gigawatt power levels and extremely high power densities. We have satisfactorily characterized the plasma flow and have achieved good agreement between measured and calculated plasma conductivities. The research work summarized in this report includes the results of our last three plasma experiments (Shots 130-5, 130-6 and 130-7), as well as the

results of a comprehensive analysis of all six plasma experiments that have used the high efficiency plasma source (Shots 130-2 through 130-7). The experimentally measured flow velocities, conductivities and other diagnostics are analyzed and compared to those predicted from hydrodynamic calculations of the plasma generation and subsequent channel flow.

The plasma source used in these latest experiments drives a 30 to 40 diameter column of high velocity, high conductivity plasma with an average hydrodynamic power on the order of a 100 gigawatts. Passing the plasma through a magnetic field of strong permanent magnets we have experimentally achieved peak MHD power densities of 3.6 terawatts/m^3-$tesla^2$.*

The objective of our next series of experiments is to demonstrate peak electrical power in the gigawatt range using an externally generated 10 tesla field. The successful completion of these experiments will demonstrate an electrical output of 3.5 kilojoules per kilogram of system weight in an expendable single pulse system. Further improvements in the output of the plasma source and configuration of the explosives can double or triple this energy output per system weight. Further increases in magnetic field

* power density in terms of the effective volume between the electrodes and the average magnetic field strength in this volume.

strength, for example by self-excitation, can yield even larger electrical power and energy outputs until extraction rates begin to seriously interact with and brake the plasma flow.

We have considered a repetitively pulsed cartridge loaded configuration and estimate an electrical output of 50 joules per kilogram of system weight per pulse for a completely contained system. The repetition rate of such a contained system would be commensurate with rapid fire gun technology and would be dependent on cartridge size.

The high power density characteristics of pulsed plasma MHD lend themselves to a number of military, research and commercial applications. Military applications include use as a prime power source in the externally or partially self-excited mode for directed energy weapons and electromagnetic guns. By virtue of their compact size and high energy and power per unit system weight, these generators are being considered as a lightweight power supply for space based weapons, surveillance and various forms of electronic warfare. These generators may also be suitable for strategic communications from low earth orbit to submerged submarines.

The pulsed plasma MHD generator can provide very high magnetic fields (in the self-excited mode) or act as a

current source for flux compressors in various research and testing applications including electromagnetic guns for hypervelocity research. On site pulse testing of large power transformers and field resistance welding of large structures have been identified as promising commercial applications.

2.0 Plasma State

In our experiments the working gas is energized at high pressures (3 GPa to 100 GPa) in a compact explosively driven device that efficiently converts the chemical energy of the explosive to the working gas/plasma. Conversion efficiencies in excess of 20% have been achieved. The plasma is then expanded down a long channel to form a high velocity extended duration pulse. The length of the plasma column is typically 30 to 40 channel diameters and the peak flow velocity is typically 25 to 30 km/s.

The argon plasma states in which we have conducted most of our experiments are shown in Figure 1 as contours of electrical conductivity on an internal energy versus pressure diagram. The conductivities are calculated using the Rogov formulation (Reference 4) based on a modified Debye-Huckel equation-of-state description. These calculations are described in further detail in References 2 and 5. The hydro code flow calculations of our plasma experiments used the 1980 Livermore argon equation-of-state (Reference 6). In the range of conditions encountered in the channel flow, the Debye-Huckel equation-of-state yields state parameters within a few percent of the Livermore equation-of-state. Thus the conductivities derived from the flow calculations using the Livermore equation-of-state are consistent.

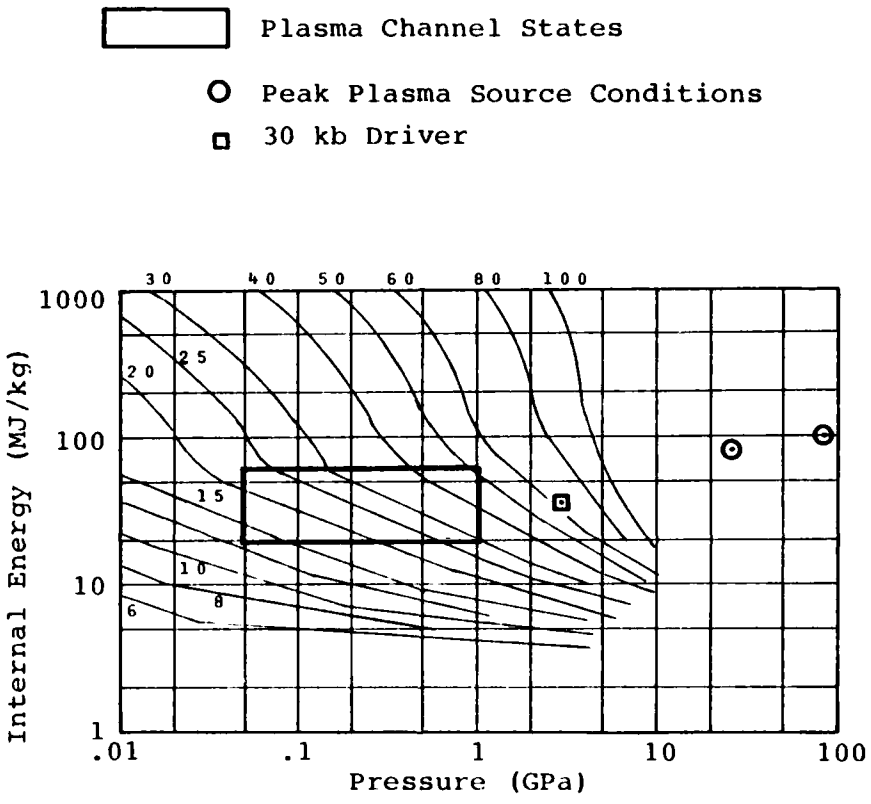

Figure 1. Argon Plasma States and Electrical Conductivity (kS/m)

The peak plasma conditions generated by the high efficiency plasma source are characterized by 100 GPa pressures and near metallic densities. In this regime the Debye-Huckel equation-of-state is not applicable and we have used only the Livermore equation-of-state to calculate plasma source dynamics.

In all of our experiments using various working gases and plasma source geometries, the bulk electrical conductivities measured or calculated in the plasma channel range from 50 kS/m at peak flow velocities of 30 km/s to 15 kS/m at the end of a highly expanded pulse. The corresponding pressure range is 1 GPa to 50 MPa. A solid theoretical foundation is essential for generating and measuring plasmas in this dense, non-ideal regime. We are confident of the 1980 Livermore equation-of-state for argon and the Rogov formulation of electrical conductivity and we are consistently getting good agreement between measured and calculated flow parameters.

Table 1 summarizes typical plasma states encountered in the plasma source and plasma channel. These estimates are based on the calculations and experiments described in Section 4.0.

		Pressure (GPa)	Energy (MJ/kg)	Density (Mg/m^3)	Conductivity (kS/m)
Plasma Source					
30 kb Driver		3	36	.295	N/A
Peak Values	Shot 130-3	85	103	2.06	N/A
End Cavity	Shot 130-7	26	81	.99	N/A
Plasma Channel					
Peak Values 17 Diameters Downstream	Shot 130-3 - Calculated	.6	49	.055	40
	Shot 130-3 - Measured	-	-	-	35
Peak Values 40 Diameters Downstream	Shot 130-3 - Calculated	.2	40.5	.023	28
	Shot 130-3 - Measured	-	-	-	22

Table 1. Typical Plasma States in the High Efficiency Plasma Source and Plasma Channel

3.0 Recent Plasma Experiments

3.1 Description of the Experiments

The high efficiency plasma source is shown in cross-section in Figure 2. Octol explosive is cast around a steel lined annular region containing a pressurized working gas. By means of the wave shaper the detonation front is caused to pass simultaneously along the outer and inner liners of the annular region. The impact of the liners forms a dynamic seal which progresses along the annulus at the explosive detonation velocity driving a strong, high pressure shock into the working gas. The result is an efficient conversion of explosive energy into the strongly shocked working gas/plasma.

The plasma converges into the hemispherical end cavity and as it stagnates it is further energized by the central piston driven by the inner core of explosive. It thereupon expands into the partially evacuated plasma channel.

Air was used as the working gas on Shot 130-5 to provide a complement to the previous work using xenon and argon. Argon was used as the working gas on Shots 130-6 and 130-7, and the end cavities were modified as shown in Figure 3. Calculations have shown that the

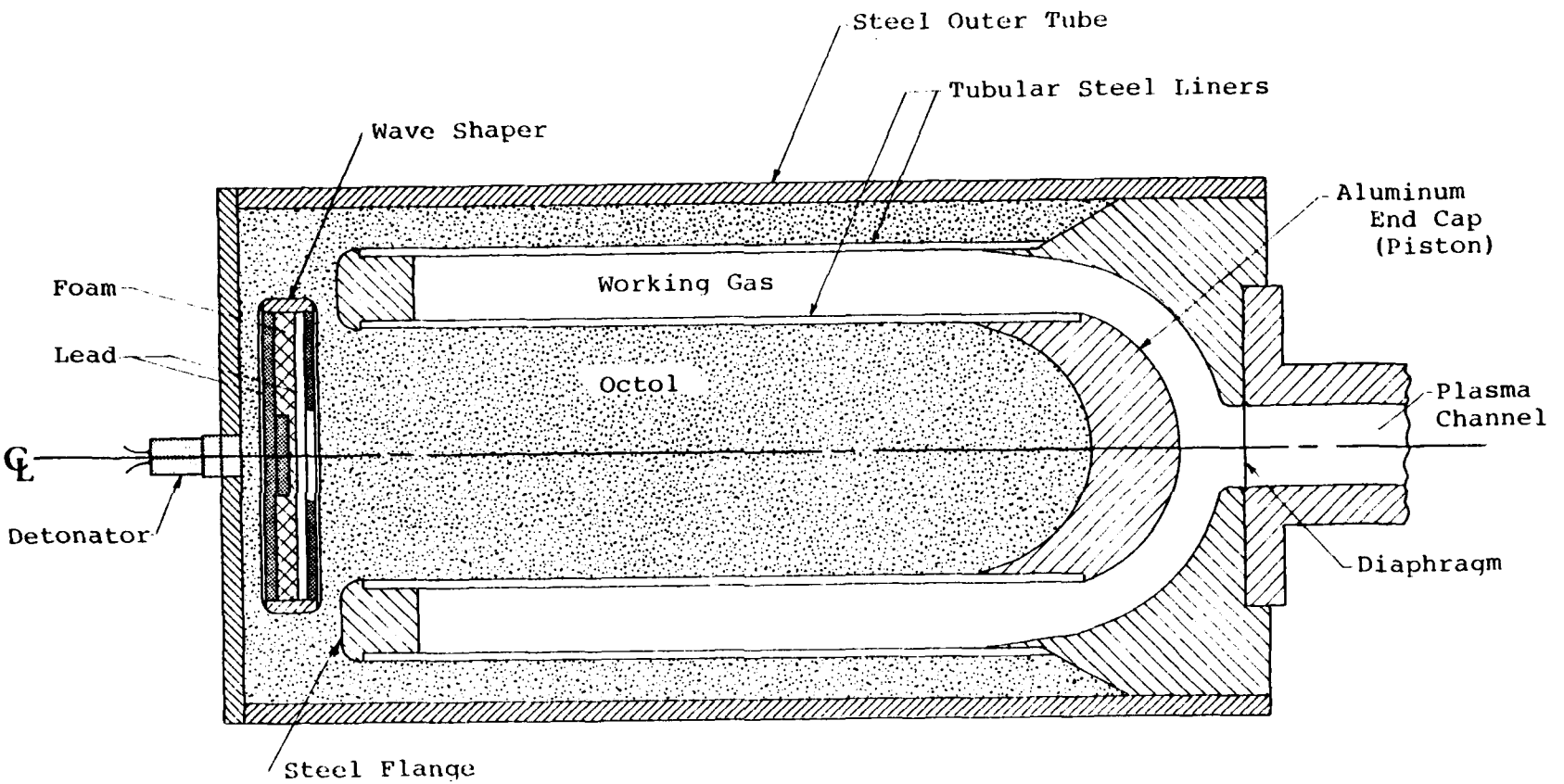

Figure 2. Cross-Section of Explosive Plasma Source

1316

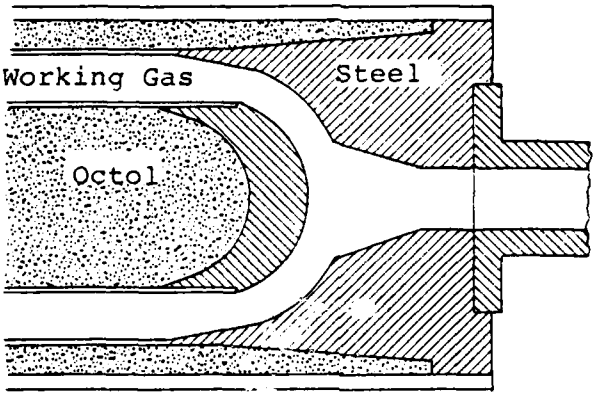

Shot 130-6

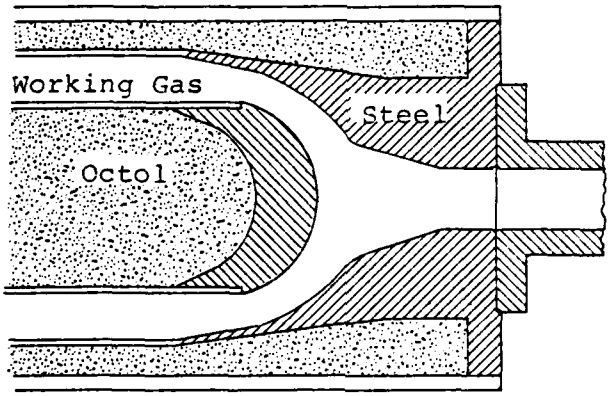

Shot 130-7

Figure 3. Modified End Cavity Sections of Explosive Plasma Sources

100 gigapascal pressures in the convergence section lead to early closure of the channel inlet. To ensure that most of the plasma is driven into the channel, the last two experiments (Shots 130-6 and 7) were designed with a short nozzle inlet connecting the cavity to the channel. Active tamping of the cavity was provided by additional explosive as shown in Figure 3.

Three types of diagnostics were used to measure the plasma properties in the channel as illustrated in Figure 4. The plasma flow velocity history was monitored by means of an open circuit Faraday generator. When a plasma passes through a transverse magnetic field, a voltage is produced. When the flow velocity, magnetic field and pick-up electrodes are mutually orthogonal, the open circuit voltage is given by

$$v_o = Bub \tag{1a}$$

where b is the interelectrode distance in meters, u is the velocity in m/s, and B is the magnetic field strength in teslas. With a known magnetic field and known electrode spacing the measured voltage provides the plasma velocity history by

$$u(t) = \frac{v_o(t)}{Bb} \tag{1b}$$

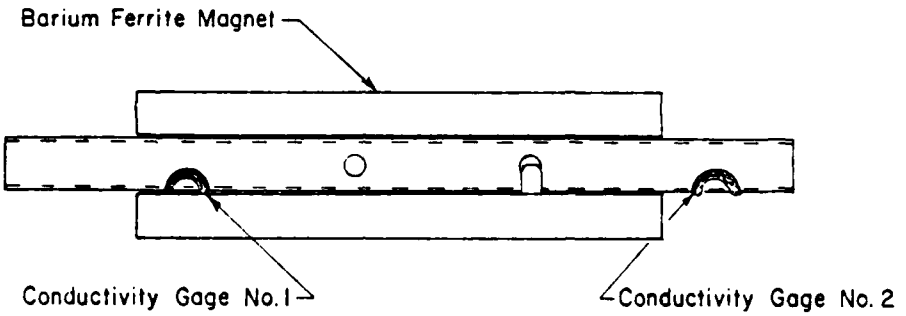

Top View

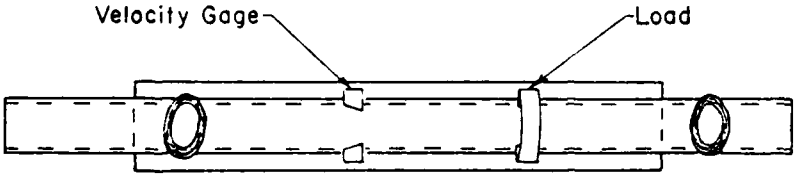

Side View

Figure 4. Typical Plasma Channel Diagnostic Station

1317

In a similar manner the plasma resistance history, and hence effective plasma conductivity, was monitored by means of a loaded Faraday generator. In this case, the generator is provided with a 10 mΩ resistive load which roughly matches the plasma resistance. The voltage appearing across the load electrodes is given by

$$v_L = v_o - R_p I - L_p \frac{dI}{dt} \tag{2}$$

where I is the load circuit current and R_p is the plasma resistance. The plasma resistance history is obtained by measuring v_L v_o, and I. V_o is obtained from the velocity gage, I is obtained from a search coil inductively coupled to the load and L_p is estimated from $\frac{dI}{dt}$ at t=0.

The effective plasma conductivity is determined from the plasma resistance by

$$\sigma = \frac{\Gamma}{R_p} \tag{3}$$

where Γ is an electrode geometry factor. This was measured in the laboratory with an electrode and channel mock-up by passing a suitable current through an electrolyte of known conductivity.

The plasma conductivity history was also measured with pickup coils placed near the magnet ends as shown.

When the plasma flows through an axial gradient in the B-field, there is an axial gradient in the induced Faraday voltage, and this results in circulating currents in the plasma. A search coil placed outside the channel will have a voltage induced in it by the time variations in the magnetic fields produced by these eddy currents. The outputs of the search coils are electronically integrated, so they directly measure the field perturbations caused by the eddy currents:

$$v = NA\Delta B/\tau \tag{4}$$

where A is coil area, N is number of turns, and τ is the integrator time constant. The magnetic field perturbation ΔB is a function of magnetic Reynolds number, being theoretically linear with R_m at low values. Thus

$$\Delta B = f(R_m) = f(\mu_o \sigma ub) \tag{5}$$

The search coils are calibrated in the laboratory by propelling a metal bar of known conductivity through a precise mockup of the shot geometry to obtain coil output as a function of magnetic Reynolds number. This, together with the measured velocity history, is used to obtain the conductivity history from the measured coil output on each shot. Further details on the design and calibration of the plasma diagnostics are given in Reference 2.

3.2 Experimental Results

The first three plasma experiments which used the high efficiency plasma source have been reported in Reference 3. These are Shot 130-2 with xenon as the working gas; Shot 130-3 with argon; and Shot 130-4 which used a scaled-up version of the 130-3 plasma source. Shot 130-1 which used a different, less energetic plasma source is not included in the present analysis. The following sections present for the first time the results of Shots 130-5, 6 and 7.

The measured flow velocity history, conductivity histories and normalized load power history for 130-5 (with air as the working gas) are shown in Figures 5, 6 and 7. The velocity history suggests a somewhat less energetic plasma than observed in previous experiments. The conductivity is initially comparable to that of previous experiments but decays more rapidly with time and with distance down the channel.

The measured load power history, like the flow velocity history, is lower than previous experiments. Based on an analysis of the plasma source data, we believe that the mass of plasma driven into the channel was less than in previous shots. The analysis in part based on the cavity X-ray (Figure 8) concludes that because of the higher shock

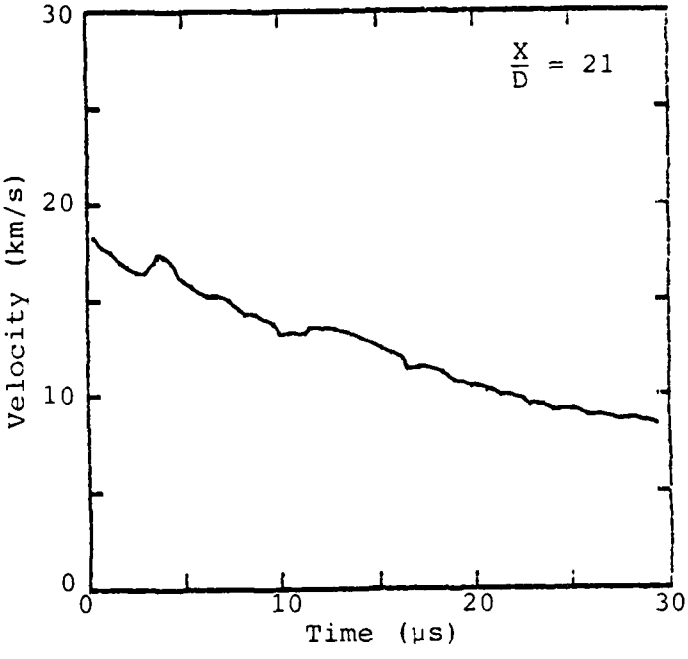

$\frac{X}{D}$ = Distance from Diaphragm in Channel Diameters

Figure 5. Flow Velocity History For Shot 130-5 (Air)

1319

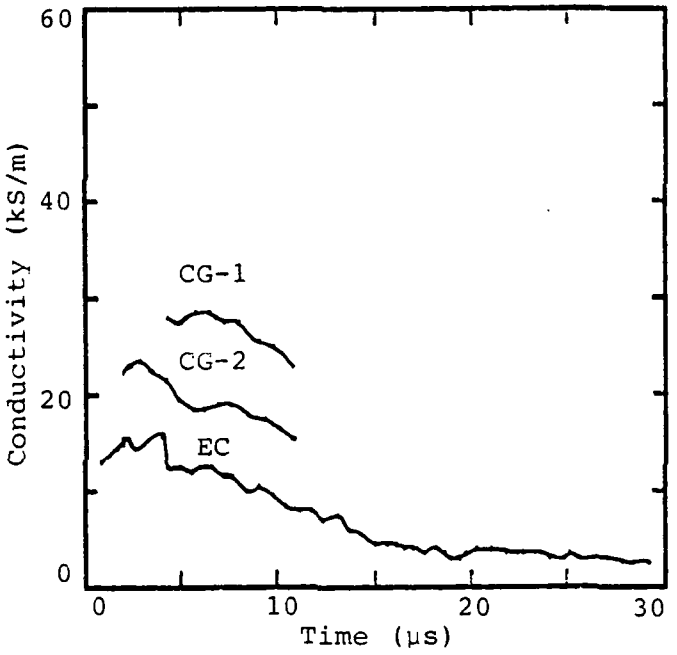

Gage	$\frac{X}{D}$
CG-1	17
EC	25
CG-2	30

CG = Search Coil Conductivity Gage

EC = Effective Conductivity From Load Electrodes

Figure 6. Conductivity Histories For Shot 130-5 (Air)

1320

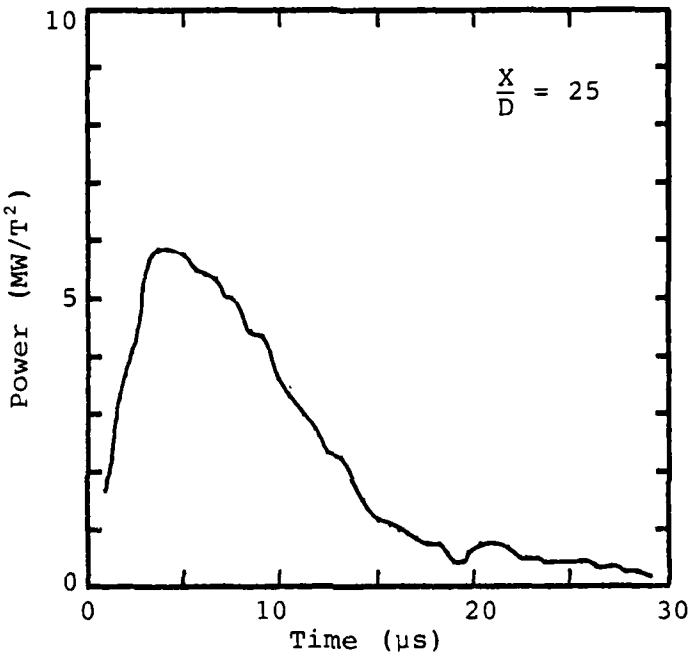

Figure 7. Normalized Load Power History For Shot 130-5 (Air)

1321

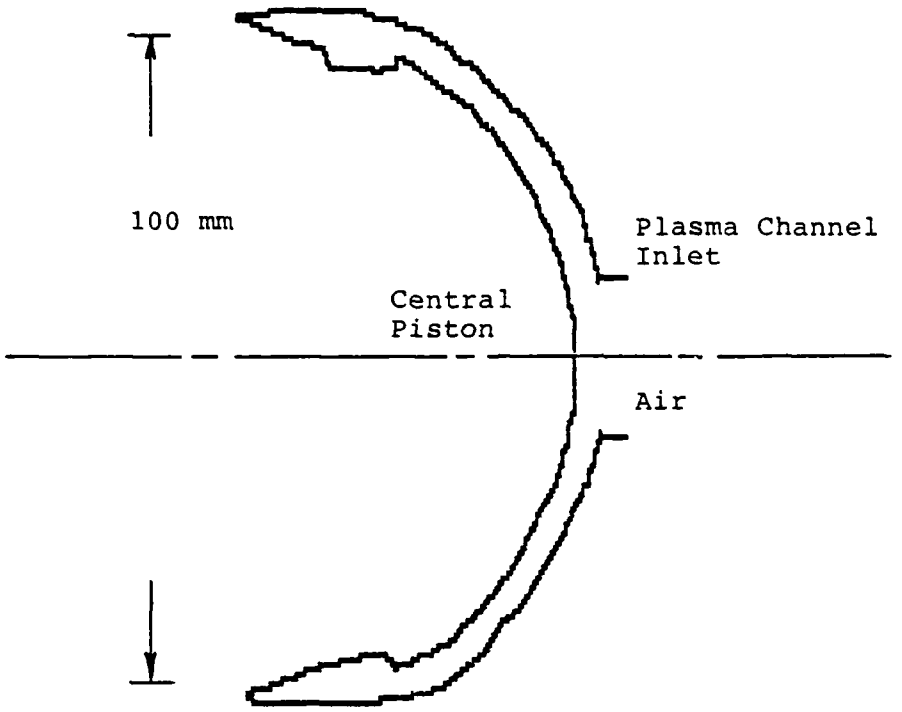

3.4 μs After First Motion of the Front
of the Central Piston

Figure 8. Digitized Representation of the
120 MEV Flash X-Ray of the 130-5
Plasma Source Cavity

1322

compressibility of air the plasma source cavity volume collapses prematurely and traps a substantial mass of plasma isolating it from the channel inlet. The plasma densities in the channel flow are therefore reduced and consequently the available hydrodynamic power is reduced.

The results for Shot 130-6 (with argon) are given in Figures 9, 10 and 11. Analysis of the cavity X-ray (Figure 12) again reveals that a substantial fraction of the plasma is trapped by a premature collision of the central piston with the cavity walls. The additional volume of the nozzle inlet results in lower cavity pressures and the central piston motion is not reversed in time. The plasma density in the subsequent channel flow is thus reduced and as a result conductivity and flow power levels are low.

The cavity for Shot 130-7 (with argon) was redesigned to force most of the plasma into the channel by eliminating the regions in the cavity where plasma can be trapped. The central piston is allowed to continue into the tapered channel inlet. This design is expected to result in a somewhat lower energy-entropy state for the plasma. The cavity X-ray (Figure 13) shows that the cavity collapsed in the manner expected.

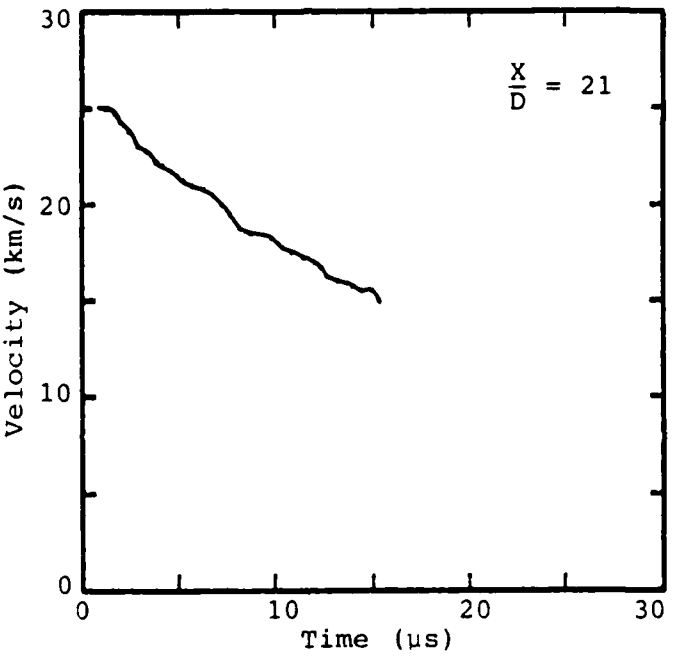

Figure 9. Flow Velocity History
For Shot 130-6 (Argon)

1323

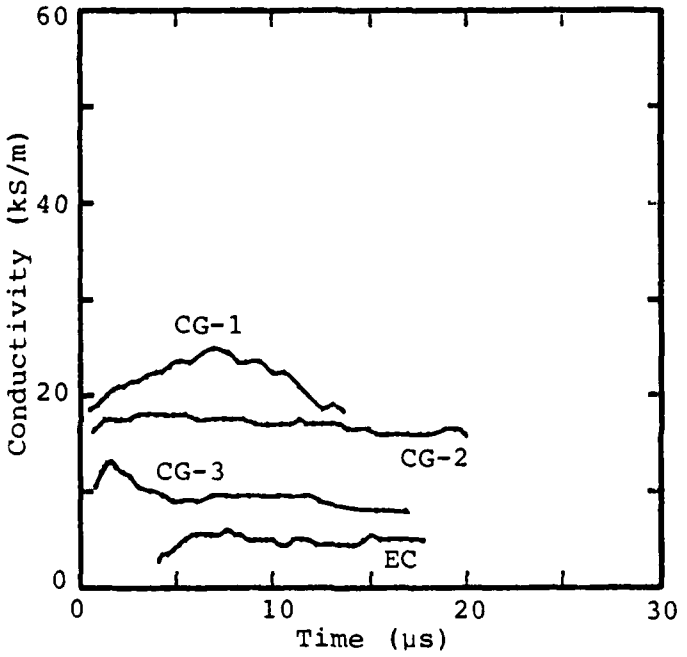

Gage	$\frac{X}{D}$
CG-1	17
EC	25
CG-2	30
CG-3	40

Figure 10. Conductivity Histories For Shot 130-6 (Argon)

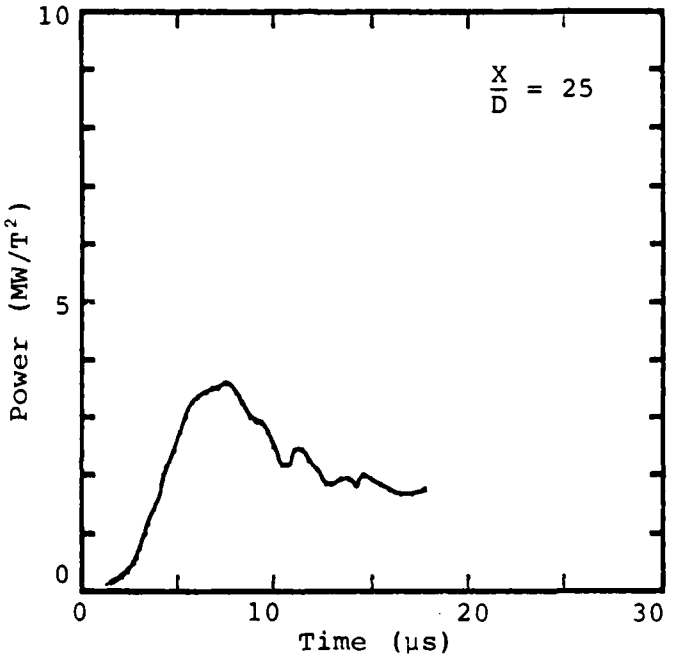

Figure 11. Normalized Load Power History For Shot 130-6 (Argon)

1325

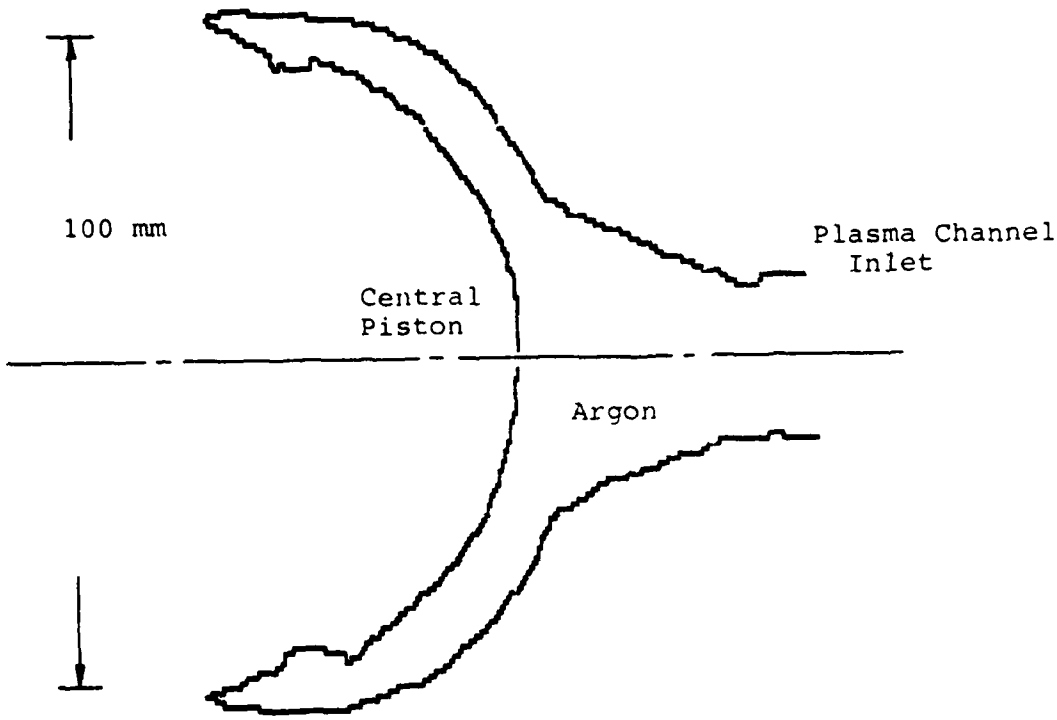

3.4 μs After First Motion of the
Front of the Central Piston

Figure 12. Digitized Representation of the 120 MEV Flash X-Ray of the 130-6 Plasma Source Cavity

1326

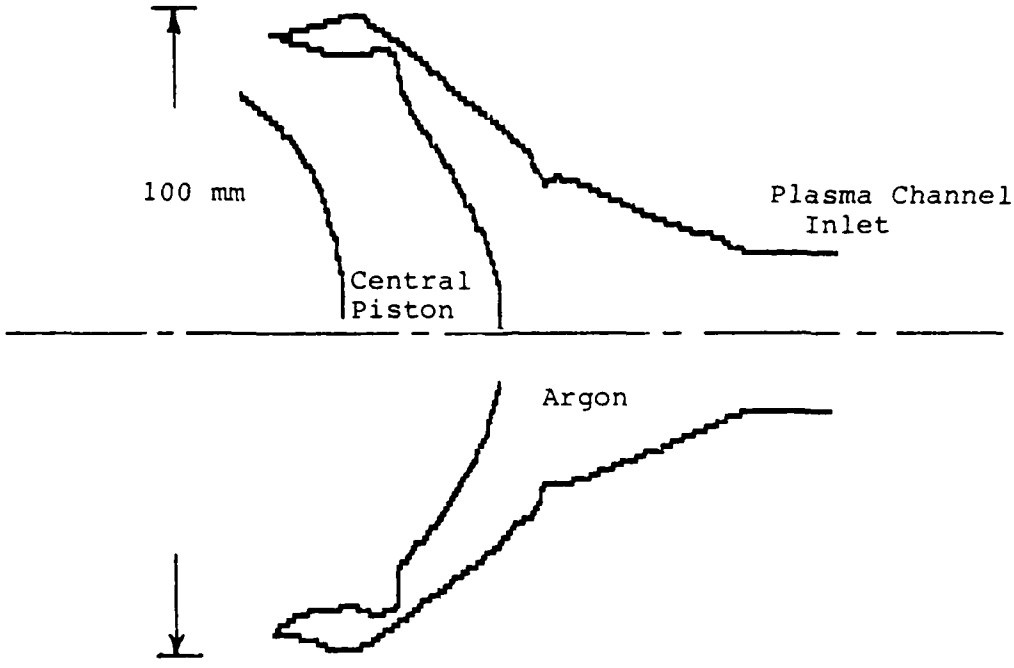

6.9 μs After First Motion of the
Front of the Central Piston

Figure 13. Digitized Representation of the 120 MEV Flash X-Ray of the 130-7 Plasma Source Cavity

1327

The results of the experiment are shown in Figures 14, 15 and 16. The general level of the velocity history is down from that of 130-2 or 130-3 in accordance with the expectation of a lower energy-entropy reservoir state. However, conductivity levels are high as would be expected with a good fraction of the source plasma driven into the channel. The effective conductivity is measured by the load electrodes and as in all previous experiments is lower than would be measured by the search coil conductivity gages. The normalized load power levels are somewhat higher than those of Shot 130-3, independently confirming the high levels of measured conductivity.

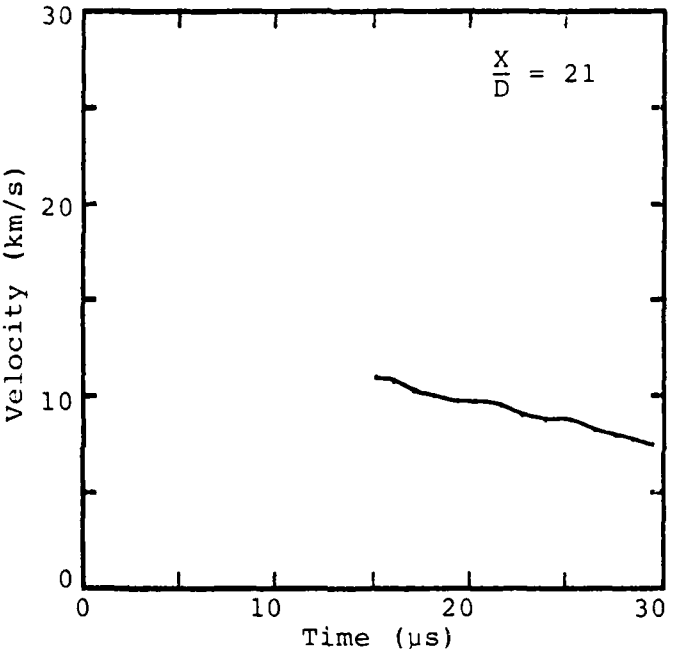

Figure 14. Flow Velocity History For Shot 130-7 (Argon)

1328

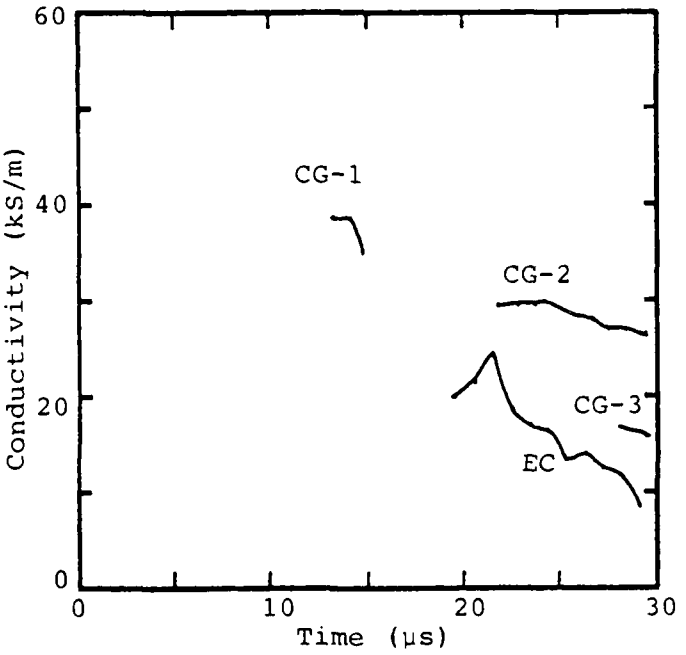

Gage	$\frac{X}{D}$
CG-1	17
EC	25
CG-2	30
CG-3	40

Figure 15. Conductivity Histories For Shot 130-7 (Argon)

1329

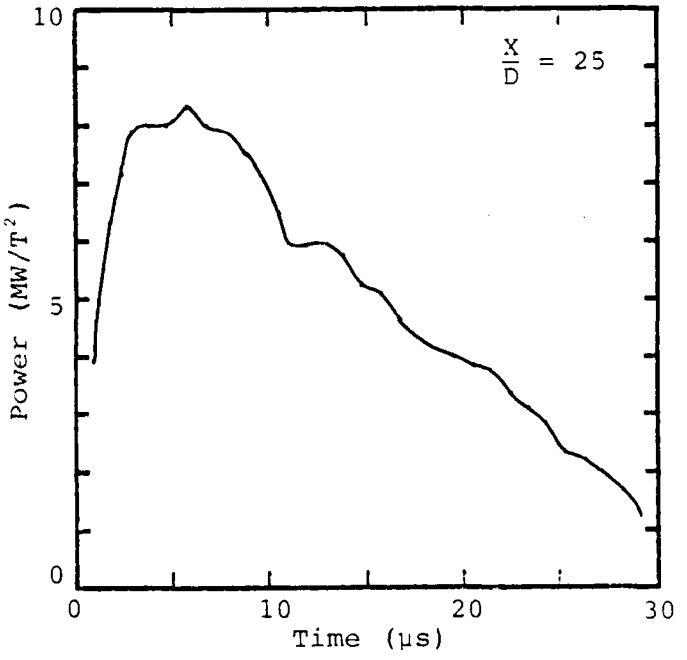

Figure 16. Normalized Load Power History For Shot 130-7 (Argon)

4.0 Analysis of Plasma Experiments

Upon completion of the three plasma experiments described in the previous section, we made a comprehensive analysis and comparison of the plasma measurements from all six shots (130-2 through 130-7) that used the high efficiency plasma source. To complement this analysis we developed a computational model for the plasma source and channel hydrodynamics and used the Rogov formulation for conductivity to estimate conductivity histories. A summary of the major parameters of the six plasma experiments is given in Table 2.

4.1 Experimental Comparisons

Three of the experiments (130-2, 3 and 5) compare three different working gases--xenon, argon and air--using otherwise identical plasma sources, plasma channels and diagnostics. The loading density of each experiment was adjusted to provide the same mass of plasma at approximately the same pressures. During the operation of the plasma source, the xenon and argon exhibit about the same compressibility. The compressibility of the air at conditions prevailing in the plasma source is significantly higher and from analysis of the plasma source diagnostics we believe that the mass of plasma driven down the channel was considerably less than in the xenon or argon experiments.

Shot	Working Gas	Plasma Source	Channel Shock Velocity (km/s)	Search Coil Conductivity After 10 μs x/D = 17 (kS/m)	Peak Load Power ($MW/Tesla^2$)	Average Load Power over 25 μs ($MW/Tesla^2$)
130-2	Xenon	Standard (Fig. 2)	26.3	37	7.16	4.28
130-3	Argon	Standard (Fig. 2)	26.4	30	8.21	4.80
130-4	Argon	1.8 Scale of Standard	30.4	50	8.39	5.26
130-5	Air	Standard (Fig. 2)	22.1	25	5.81	2.44
130-6	Argon	Modified (Fig. 3)	27.9	22	3.54	-
130-7	Argon	Modified (Fig. 3)	26.6	40	8.26	5.48

Table 2. Summary of Plasma Experiments Using the High Efficiency Plasma Source (3 GPa Driver)

This conclusion is further strengthened by the lower flow velocity and normalized load power observed in the plasma channel. Otherwise these three experiments represent a comparison of the conductivities of the three working gases.

The measured flow velocity histories, conductivity histories and normalized load power histories for the three shots are shown in Figures 17, 18, 19 and 20. Xenon conductivities average about 30% higher than those of argon. Based on our best estimates and taking account of plasma source performance, it appears that air conductivity may be as high or higher than that of argon at the same thermodynamic conditions.

The channel shock velocities for all six experiments are listed in Table 2. From previous work (Reference 7) we have noted that framing camera records of the flow have often shown a highly canted non-uniform shock front. At least the first few diameters of channel flow is not one-dimensional and for this reason we have made no attempt to relate the peak measured flow velocity to the one-dimensional Hugoniot flow velocity for the observed shock velocity.

In 130-4 the dimensions of the plasma source were scaled by a factor of 1.8 over those of 130-3. The channel and diagnostics were unchanged. The objective of 130-4 was

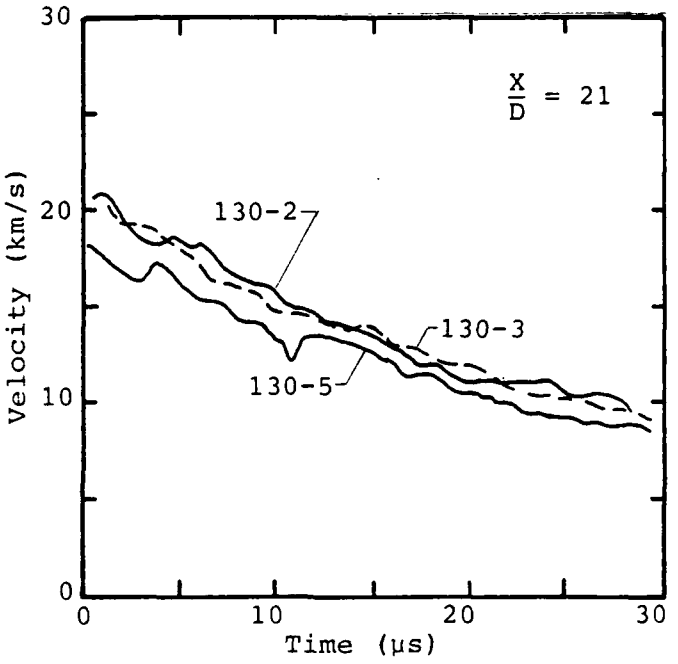

Shot	Working Gas
130-2	Xenon
130-3	Argon
130-5	Air

Figure 17. Flow Velocity Histories For Shots 130-2, 3 and 5

1331

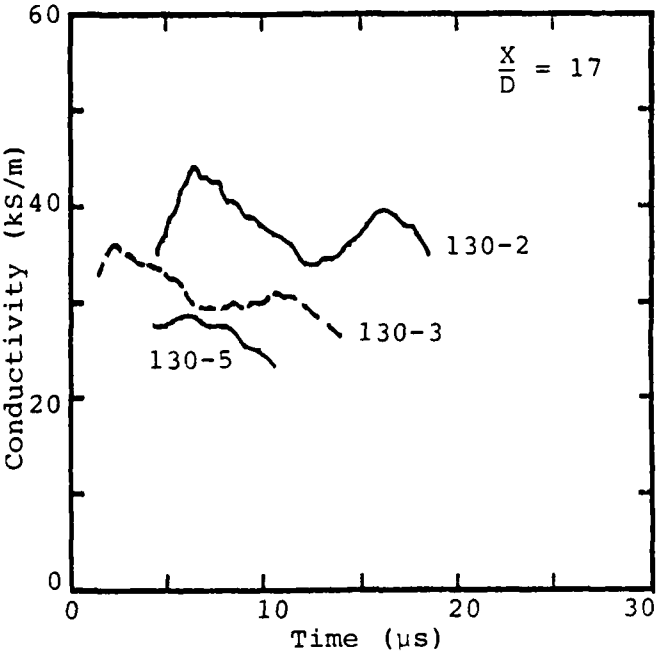

Shot	Working Gas
130-2	Xenon
130-3	Argon
130-5	Air

Figure 18. Conductivity Histories For Shots 130-2, 3 and 5 (Conductivity Gage 1)

1332

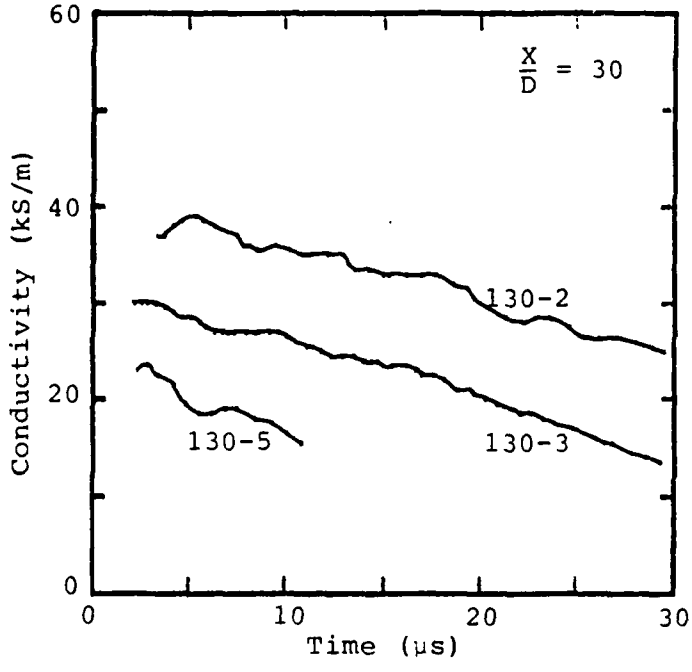

Shot	Working Gas
130-2	Xenon
130-3	Argon
130-5	Air

Figure 19. Conductivity Histories For Shots 130-2, 3 and 5 (Conductivity Gage 2)

1333

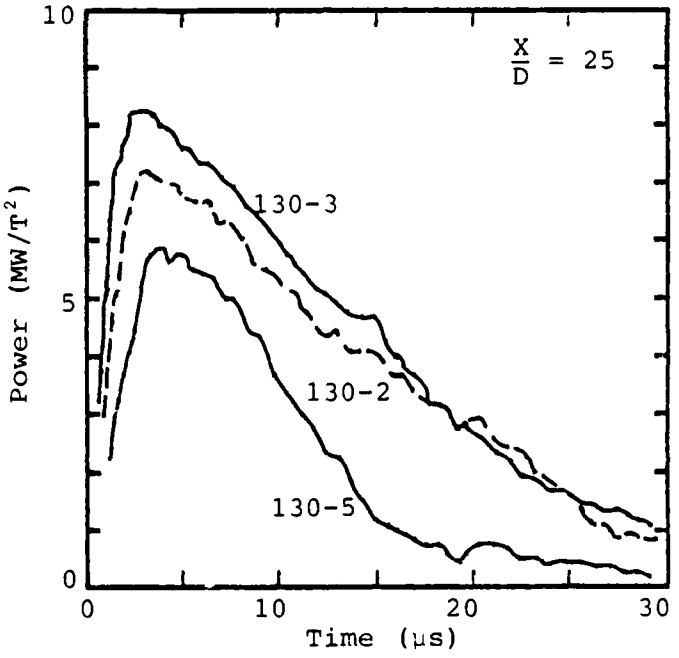

Shot	Working Gas
130-2	Xenon
130-3	Argon
130-5	Air

Figure 20. Normalized Load Power Histories For Shots 130-2, 3 and 5

1334

to extend the duration of channel flow by increasing the duration of the high channel inlet conditions. The velocity, conductivity and normalized load power histories for the two experiments are shown in Figures 21, 22 and 23 and it is evident that performance gains with the larger source are modest. There are two leading hypotheses to account for this.

1. The channel inlet is collapsed by the 85 GPa plasma source pressures thereby cutting off the plasma flow at approximately the same time in both experiments. This effect is predicted and roughly quantified by the 2-D code calculations supporting the Lawrence Livermore Voitenko compressor experiments (Reference 8) which gave peak channel inlet conditions very close to our experiments.

2. Boundary layer growth in the high pressure region of the channel near the plasma source is driven by wall ablation and closes within 10 to 20 diameters of the shock front. We are currently incorporating boundary layer effects into our flow calculations to determine whether the flow conditions just downstream of the plasma source can generate a sufficiently blown boundary layer to affect the flow in the ways we observe.

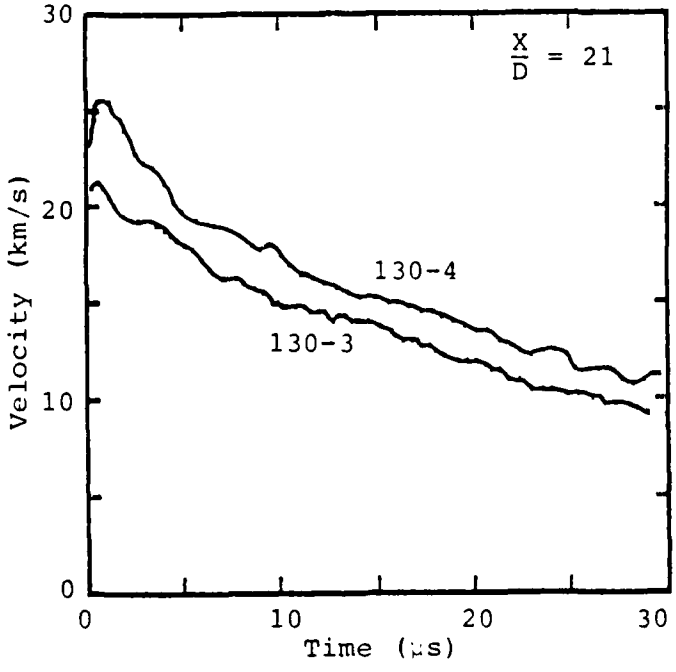

Figure 21. Flow Velocity Histories For Shots 130-3 and 4

1335

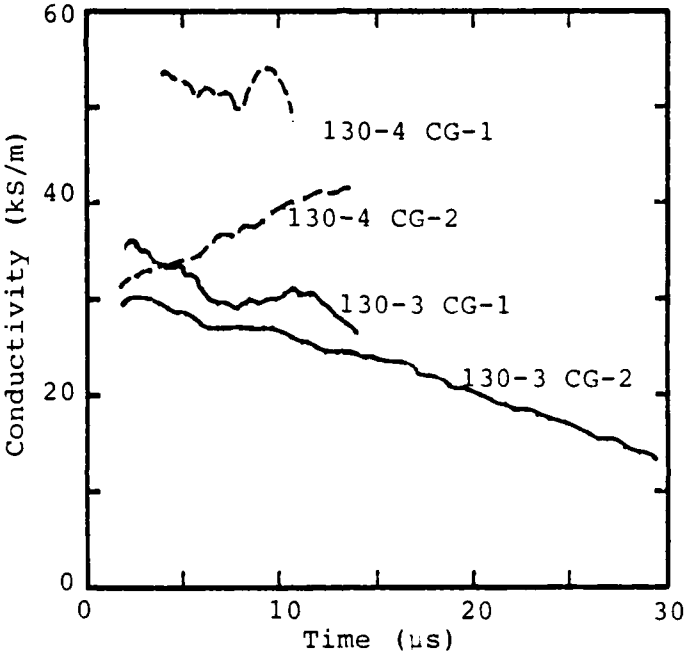

Gage	$\frac{X}{D}$
CG-1	17
CG-2	30

Figure 22. Conductivity Histories For Shots 130-3 and 4

1336

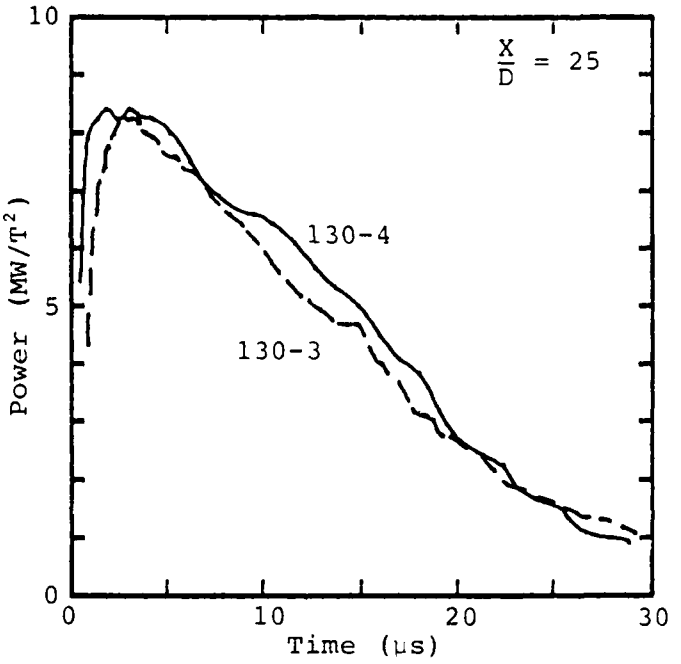

Figure 23. Normalized Load Power Histories For Shots 130-3 and 4

1337

The plasma source used in the 130-7 experiment represents an improvement in the design of the end cavity and channel inlet. The comparison of channel diagnostics for 130-3 and 130-7 (Figures 24, 25 and 26) illustrates the effect of these changes. As judged by conductivity and load power histories the improvements in channel flow conditions are modest even though an analysis of the plasma source cavity collapse would indicate that considerably more plasma has to be driven into the channel. The relative insensitivity of pulse duration to improvements in plasma source design may be another indication of channel flow controlled by blown boundary layer effects.

As reported in our previous work (References 1, 2 and 3) the conductivity measured by the search coil conductivity gages is invariably higher than the effective plasma conductivity calculated from the load electrode current and voltage traces. The conductivity gage measures the magnetic flux from eddy currents within the plasma and therefore tends to weight the regions of higher conductivity. The effective conductivity derived from load electrode measurements, however, would tend to weight the more resistive boundary layer regions and be responsive to the details of electrical contact between plasma and electrodes. We continued to observe this difference in Shots 130-5 through 130-7. We use the lower and more relevant effective conductivity values in our estimates of MHD power generation.

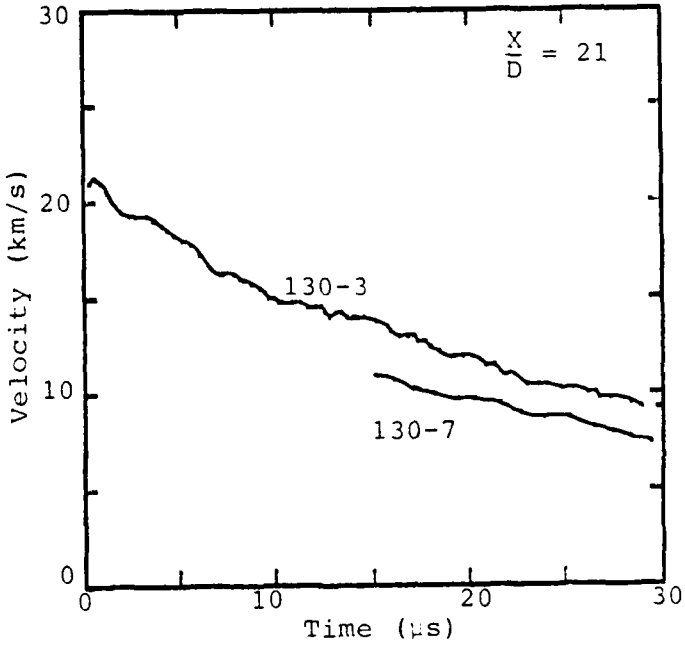

Figure 24. Flow Velocity Histories For Shots 130-3 and 7

1338

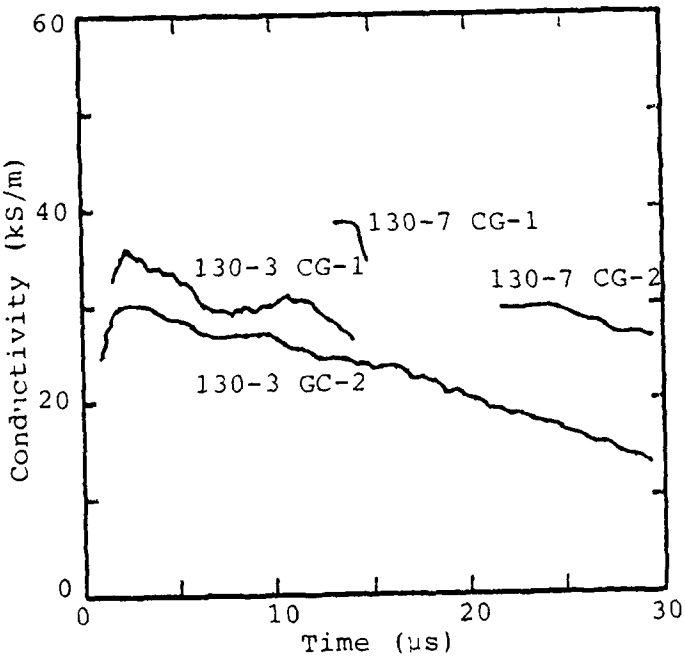

Gage	$\frac{X}{D}$
CG-1	17
CG-2	30

Figure 25. Conductivity Histories For Shots 130-3 and 7

1339

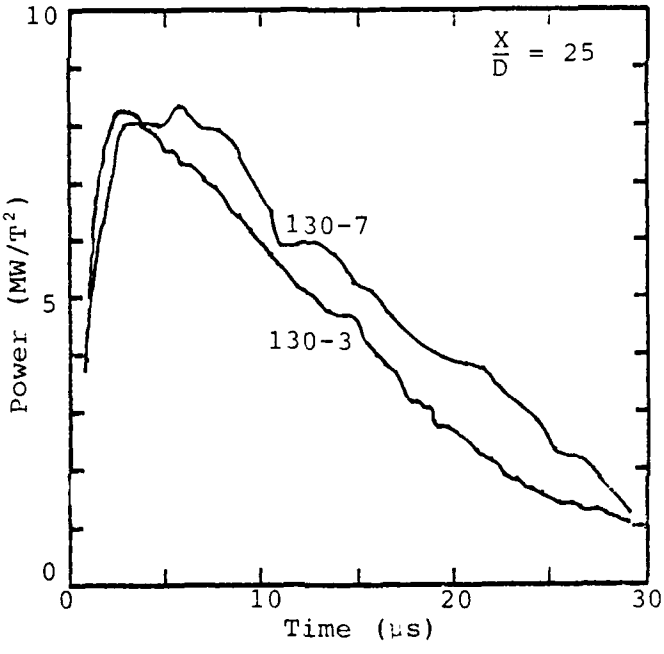

Figure 26. Normalized Load Power Histories For Shots 130-3 and 7

340

The normalized load power curves such as shown in Figures 23 and 26 are derived by multiplying the measured load current by the measured voltage then dividing by the square of the measured magnetic field strength. The generation volume as defined by the plasma volume accessible to the load electrodes is 2.3 cm^3. For Shot 130-7 the peak normalized power density is 3.6 $TW/m^3\text{-}T^2$ (Figure 16) and the normalized power density averaged over the first 25 us of flow is 2.4 $TW/m^3\text{-}T^2$.

While this power density was measured for a field strength of about 0.1 tesla we expect that it will be reasonably constant up to field strengths of at least 10 tesla. Much of this confidence is based on the high currents and field amplifications observed in previous work on self-excitation (References 2, 3 and 9). Current in the self-excited shot increased as expected until the process quenched as a result of the limited pulse length.

Consider a resistive and inductive load circuit with the current given by the relation

$$(L_L + L_p)\frac{dI}{dt} + (R_L + R_p)I - \text{Bub} = 0 \qquad (6)$$

and the load voltage by

$$V_L = L_L \frac{dI}{dt} + R_L I \qquad (7)$$

For load and plasma inductances typical of our experiments, the inductive voltage drop can be neglected after the first few diameters of flow. Thus, for a matched load, the load power is

$$P_L = V_L I$$
$$= \frac{(Bub)^2}{4R_L} \qquad (8a)$$

Expressing the plasma resistance in terms of conductivity, the load power becomes

$$P_L = \frac{B^2 u^2 b A \sigma}{4}$$
$$= \frac{B^2 u A R_m}{4\mu_o} \qquad (8b)$$

where $R_m = \mu_o \sigma u b$ (magnetic Reynolds number)

and A = effective electrode area

For a 10 tesla field, large electrodes and an average R_m of 10 (typical of our experiments), the average electrical power extracted would be 10 gigawatts with a peak of nearly twice this value. The average electrical power extracted is about 10% of the average hydrodynamic power available in the flow and might be expected to cause moderate flow perturbations.

4.2 Calculation of Channel Flow and Conductivity Histories

4.2.1 Calculational Method

We have utilized an advanced 1½-D hydro code with interactive wall motion to model the energizing of the plasma and subsequent channel flow. The collapse of the plasma source cavity is made to conform closely to a number of experimentally observed constraints. This approach is valid because of the high sound speeds characteristic of the plasma in the source. It gives a good account of overall flow dynamics and allows a rapid evaluation of parameters controlling the flow.

Our calculations are based on the 1-D streamtube finite difference equations of Reference 10. The working gas is modeled by a 28 term polynomial fit to the 1980 Livermore argon equation-of-state (Reference 6) and is the best available data for the entire range of plasma states encountered in the plasma source and subsequent channel flow. The channel is modeled by a series of wallpoints (Figure 27) whose radial motion is controlled by the local channel pressure and by the shock Hugoniot characteristics of the material associated with the wallpoints. Channel wallpoints at diagnostic locations corresponding to those of the experiments are used to collect the appropriate

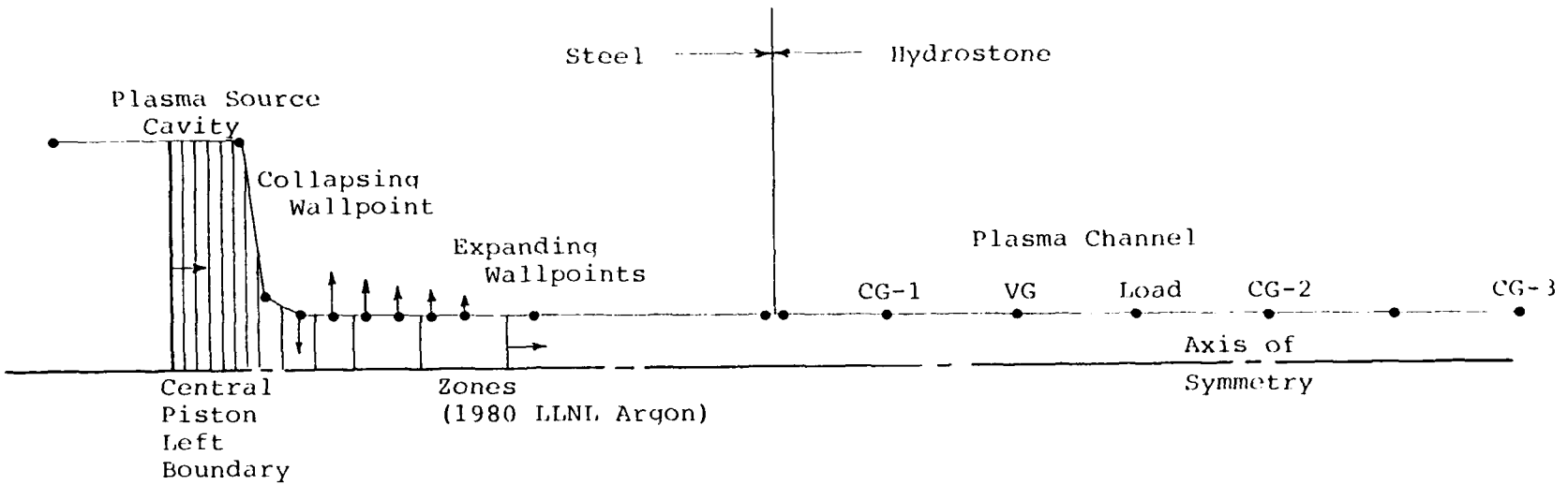

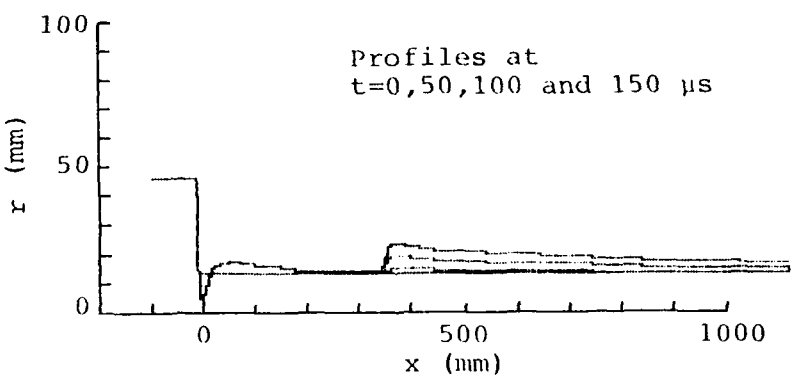

Calculated Wall Motion for Shot 130-3

Figure 27. Schematic of the 1½-D Hydro Code Calculations with Interactive Wall Motion

hydrodynamic variable data for direct comparison. In the case of conductivity gage locations, the pressure and internal energy histories are saved and used in a post-processor code to compute a conductivity history based on a table lookup compiled from the Rogov formulation of plasma conductivity (References 4 and 5). Load voltage and current are also computed by the post-processor code from a saved velocity history and derived conductivity history. These histories are used in a numerical solution of the load circuit equation (6) to derive current and voltage histories.

The air in the channel ahead of the working gas is modeled by an air Hugoniot boundary condition.

Modeling the operation of the plasma source is the key to achieving a reasonable channel flow calculation. Referring to Figure 27, the calculation is begun when the central piston first begins to move. The state of the working gas in the cavity is determined fully by specifying two state variables. The density of the gas is calculated from the volume of the cavity and the estimated mass of gas in the cavity. The entropy of the gas is assumed to be that of the driver gas when brought to rest by a strong shock reflection. The initial cavity state is then taken to lie on the isentrope passing through this reflected

shock state. The motion of the central piston in the cavity begins when the shock, driven by the core explosive, reaches the front surface of the piston. In our calculations, this initial motion is prescribed based on an analysis of a high speed framing camera record of the piston motion from a separate experiment (Reference 7). The proper momentum of the piston is estimated from a 1½-D hydro code calculation of the central core explosive event. When the gas arrives in the cavity, typically 1 to 2 μs after first motion of the piston, the motion of the piston is therafter determined by the difference in pressure across the piston. The initial cavity volume is chosen from an analysis of cavity X-ray data. The cavity walls in the calculation are configured to give the approximate volume as a function of time determined from cavity X-ray data. Thus the energization of working gas in the cavity is closely linked to the available experimental data.

With the initial conditions and boundary conditions so constrained, the mass of working gas is the remaining parameter to be selected. In all our experiments we begin with about 60 grams of gas in the system. From many prior tests we estimate about 5% of this is lost in the driver start-up process. From cavity X-rays, we estimate a further loss in the region where the gas enters

the end cavity (see Figure 8 for example). The remaining gas--usually 25 to 35 grams--is considered available for processing in the cavity. In the case of 130-3 we believe the inlet to the plasma channel collapses rapidly cutting off the flow of gas to the channel and further reducing the mass of working gas. This collapse process is modeled by using a collapse trigger level and radial collapse history based on the 2-D code calculations of the Voitenko compressor (Figure 28) and scaled appropriately for our geometry.

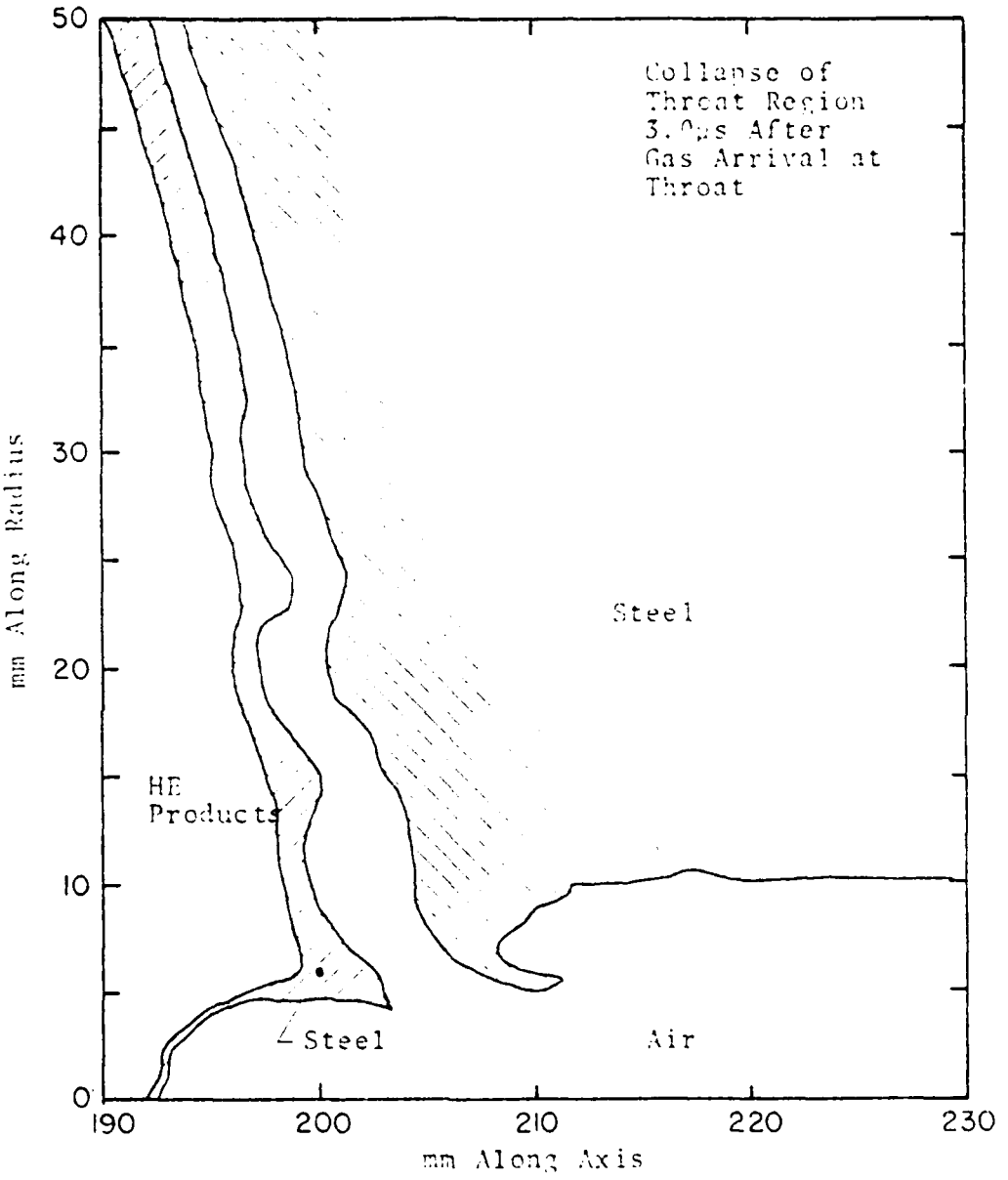

Figure 28. Calculation of the Voitenko Generator (Reference 8)

342

4.2.2 Comparison of Calculated and Measured Results

The calculated and measured flow velocity and conductivity histories for 130-3 are shown in Figures 29 and 30. The calculated velocity is higher than the measured velocity and several reasons may be cited.

1. The initial entropy state of the source plasma assumed in the calculations may be too high since the plasma is probably processed in the cavity by multiple shocks rather than one strong shock.

2. The early values of the measured velocity may be lower than the calculated 1-D velocity because of the non-uniformity of the flow and the manner in which the velocity gage averages the flow.

3. At later times, wall expansion could change the velocity gage electrode spacing and magnetic field thus invalidating the gage calibration.

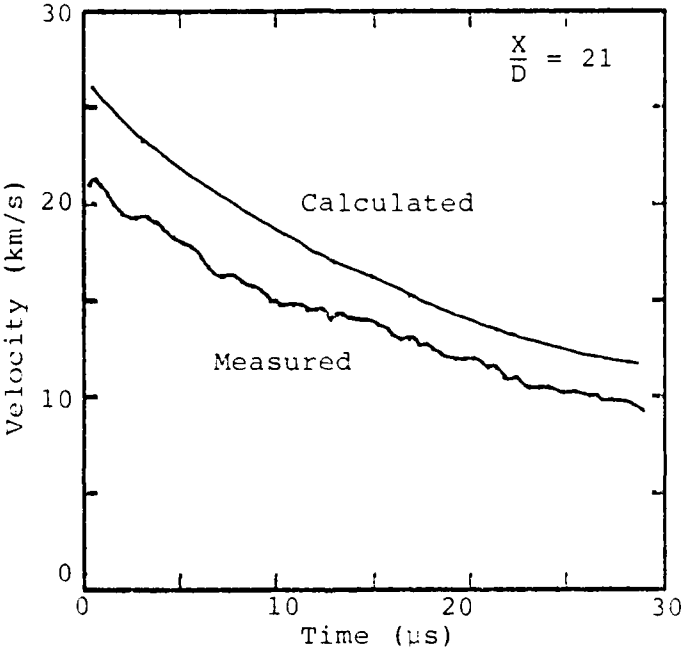

Figure 29. Calculated and Measured Flow Velocity Histories For Shot 130-3

343

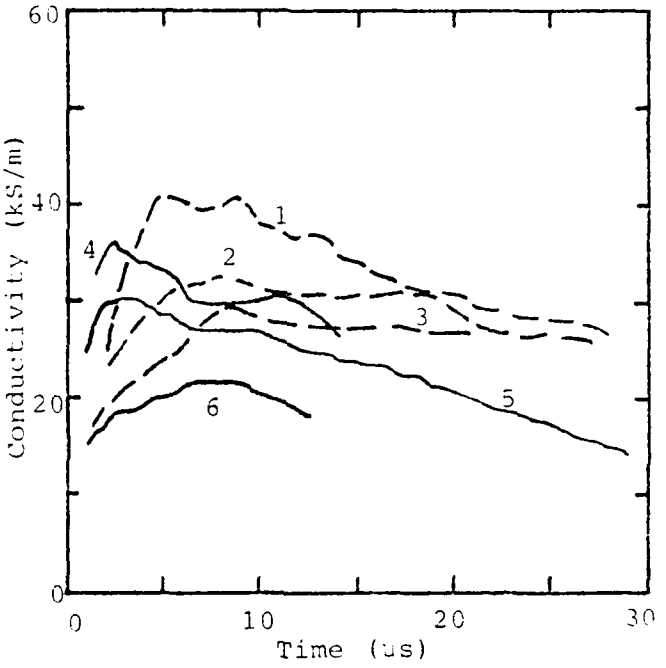

1. $\frac{X}{D} = 17$
2. $\frac{X}{D} = 30$ } Calculated
3. $\frac{X}{D} = 40$
4. $\frac{X}{D} = 17$
5. $\frac{X}{D} = 30$ } Measured
6. $\frac{X}{D} = 40$

Figure 30. Calculated and Measured Conductivity Histories For Shots 130-3

4. Boundary layer growth and flow contamination are not included in the calculations and if important would tend to reduce the calculated velocity at late times.

It was noted during the course of several calculations that the calculated velocity was insensitive within limits to the mass of plasma initially assumed to be available for processing in the plasma source cavity. However, lowering the initial entropy state assumed for the calculations would directly lower the calculated velocity since the flow velocity is determined primarily by the energy density of the reservoir gas.

The calculated form of the conductivity histories and decay of peak conductivity with distance reasonably reflect the observed behavior. The calculated plasma pressure and internal energy histories are given in Figures 31 and 32 and can be used to find the other state variables in the 1980 Livermore equation-of-state for argon. In the calculation 14 grams of plasma are driven into the channel before the inlet is completely collapsed. The effect of wall expansion can be gaged by noting that the total enthalpy of the plasma pulse measured at any point along the diagnostic channel remains constant at 2.1 MJ. Wall motion is too slow to

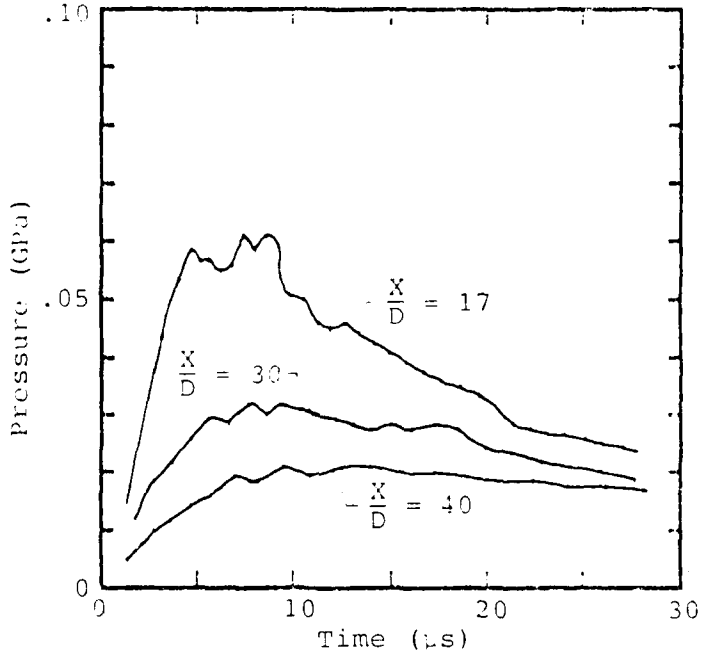

Figure 31. Calculated Pressure Histories For Shot 130-3

1347

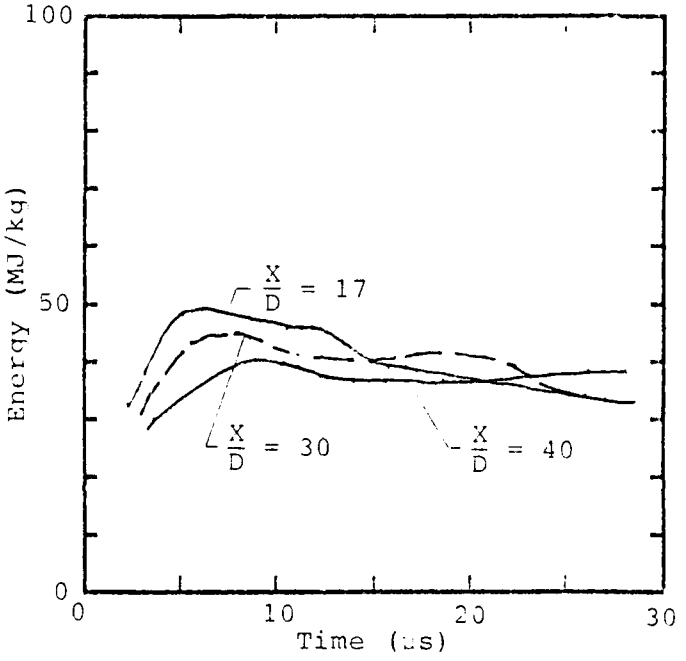

Figure 32. Calculated Internal Energy Histories For Shot 130-3

significantly degrade the energy of the pulse since it is concentrated at the high velocity leading edge of the pulse. The compression of the plasma in the cavity by the central piston is nearly isentropic to a peak of 85 GPa. Although this compression is extremely impulsive (Figure 33), the plasma enters the cavity at a high entropy level from the strong shock driver process and shock Mach numbers in the cavity are never high.

The calculated and measured flow velocity and conductivity histories for the modified plasma source of 130-7 are shown in Figures 34 and 35. The agreement is fair although the calculated velocity is again higher for the same reasons cited previously. In the calculation the channel inlet is not forced to collapse and 20 grams of plasma are driven into the channel resulting in considerably higher plasma densities than calculated for the 130-3 experiment. The computed flow velocity is slightly lower than that of 130-3 and the calculated conductivity histories are in general slightly higher than those of 130-3. Peak computed cavity pressure is 25 GPa, less than one third of that calculated for 130-3.

The X-ray of the cavity collapse of 130-6 indicates that a substantial mass of plasma is trapped by a premature collision of the central piston with the cavity

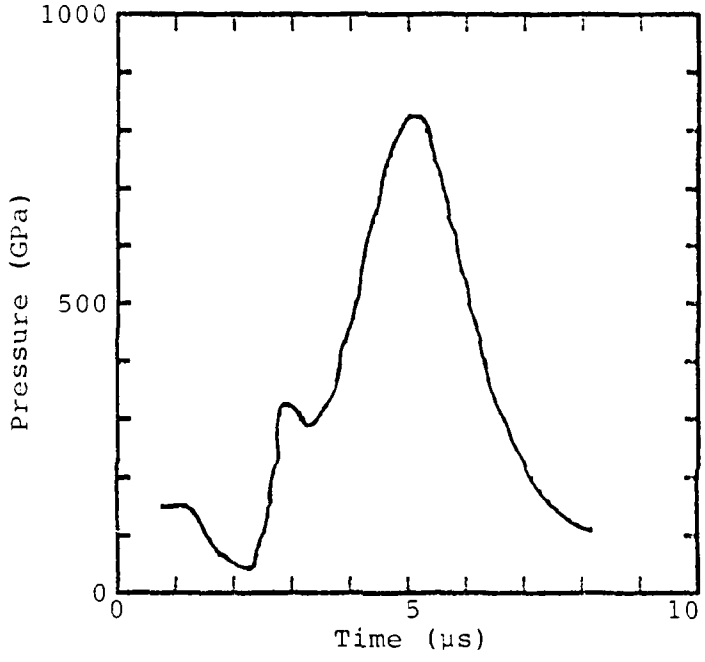

Figure 33. Calculated Cavity Pressure History For 130-3

1349

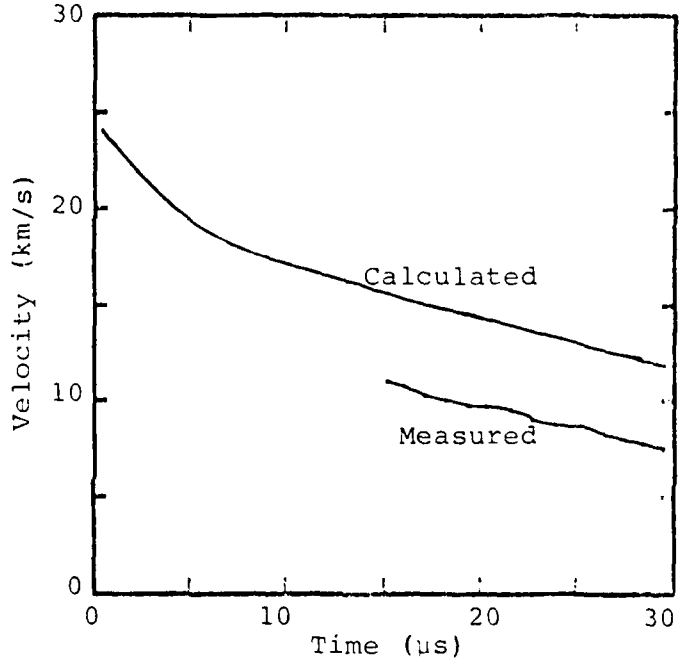

Figure 34. Calculated and Measured Flow Velocity Histories For Shot 130-7

1350

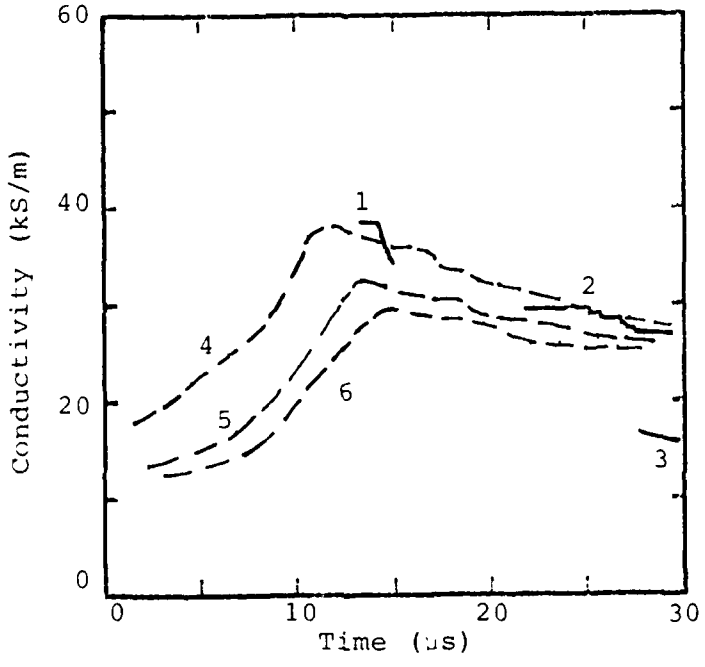

1. $\frac{X}{D} = 17$
2. $\frac{X}{D} = 30$
3. $\frac{X}{D} = 40$

} Measured

4. $\frac{X}{D} = 17$
5. $\frac{X}{D} = 30$
6. $\frac{X}{D} = 40$

} Calculated

Figure 35. Calculated and Measured Conductivity Histories For Shot 130-7

/351

walls. In the calculation it was necessary to reduce the mass of plasma entering the channel to about 8 grams to achieve reasonable agreement with the observed flow velocity and conductivity histories. The low level of conductivity is directly related to the low average gas density in the channel.

When the mass of plasma in the channel is in rough agreement with the mass expected from analysis of the cavity X-rays, the agreement between calculation and experiment is reasonable. The calculations depend strongly on the source modeling, on the validity of the equation-of-state and on the applicability of the Rogov formulation of conductivity. Because of the good agreement with measured results, we are confident of all three choices. Channel pressure history measurements are planned for future experiments to provide additional confirmation of our hydrodynamic calculations.

In future calculations we plan to incorporate ablative boundary layer effects into the description of channel flow. As this effort progresses we expect to gain additional insights into the hypothesis that early closure of a blown boundary layer can have a limiting effect on the duration of the plasma pulse. We are also planning to add an MHD power extraction model to the code to begin to determine the overall effects of high power

extraction on the braking of the plasma flow. We also plan to review the choice of initial plasma state assumed in the source cavity. We are considering a 2-D axisymmetric hydro calculation to more accurately assess the processes by which the plasma enters the cavity, converges on-axis and flows into the channel.

5.0 Conclusions and Recommendations

5.1 Summary of Program Accomplishments

- We have generated and measured plasma conditions of extremely high energy, electrical conductivity and flow velocities. Using a high efficiency plasma source we have achieved flow velocities of 30 km/s with electrical conductivities as high as 50 kS/m.

- An excellent analytical framework for describing the plasma states has been established. The 1980 Livermore equation-of-state for argon is now used to describe the thermodynamic states encountered in the plasma source and channel flow. The Rogov formulation for electrical conductivity is used for the plasma states characteristic of the channel flow.

- A 1½-D hydrodynamic code technique has been used to model the plasma energization and subsequent channel flow. Using the calculated hydrodynamic flow histories and the Rogov formulation for conductivity, we have achieved satisfactory agreement between calculated and measured conductivity histories for argon plasmas.

- In the channel flow plasma states characteristic of our experiments, the range of measured electrical conductivities varies from 50 kS/m at peak conditions to 15 kS/m at the end of the highly expanded plasma pulse. Xenon exhibits a somewhat higher conductivity than argon or air at the same thermodynamic state.

- As noted in previous experiments, measured interelectrode plasma resistance is higher than that calculated from bulk (search coil) conductivity measurements. This difference is tentatively ascribed to differences in the averaging process by the two measurement techniques in the presence of a less conductive boundary layer.

- The duration of the plasma pulse is relatively insensitive to source size and source geometry. We hypothesize that pulse duration may be limited by early closure of a blown boundary layer in the high pressure region of the channel near the plasma source.

- Based on hydro code calculations that agree with measured flow velocities and conductivities, we estimate a peak flow enthalpy of a terawatt at

the source exit and 0.2 terawatts in the plasma diagnostic section of the channel. The total enthalpy of the plasma pulse in the channel is approximately 2.5 MJ.

- We have measured peak electrical power densities of 3.6 $TW/m^3\text{-}T^2$ using small electrodes in a field provided by permanent magnets. The average power density over the first 25 us of the plasma is 2.4 $TW/m^3\text{-}T^2$. With the flow conditions already achieved we are confident of extracting electrical power at levels of tens of gigawatts in a 25 mm channel with an externally produced 10 tesla field.

A summary of the plasma parameters achieved in this program is given in Table 3.

Peak Plasma Source Conditions

Plasma Pressure	-	85 GPa
Specific Energy	-	100 MJ/kg
Flow Power at Channel Entrance	-	1 TW

Peak Channel Conditions (at 20 diameters)

Flow Velocity	-	30 km/s
Conductivity	-	50 kS/m
Flow Power	-	0.2 TW
Total Pulse Enthalpy (40 μs pulse)	-	2.5 MJ
Peak Electrical Power Density	-	3.6 TW/m^3-T^2
Average Electrical Power Density (over 25 μsec)	-	2.4 TW/m^3-T^2

Table 3. Summary of Achieved Performance in Plasma Source and 25 mm Channel

5.2 Recommendations

- We recommend plasma experiments using an externally applied magnetic field on the order of 10 tesla to achieve high electrical power output and to investigate the moderate plasma flow interactions resulting when over 10% of the available hydrodynamic power is extracted.

- Measurement of channel flow pressure histories are recommended to provide further confirmation of channel plasma conditions.

- Investigations should be continued on the limiting effect of a blown boundary layer on the pulse duration of plasma flow in the channel. This analysis may also help clarify the effect of boundary layer growth on interelectrode resistance.

- Further development of the plasma source should be undertaken to increase the mass of plasma driven into the channel since increased flow densities directly increase the level of plasma conductivity.

- Continued development of the 1½-D computations are recommended to model the overall effects of MHD power extraction on the plasma flow and its thermodynamic state.

- A program to study the detailed 3-D interactions of the plasma flow, magnetic field and electrical power extraction circuit should be initiated to form the basis of a fully interactive 3-D MHD computer code.

References

1. Gill, Stephen P. et al, "Explosive MHD Research," Artec Associates Incorporated, Annual Report 119, Navy Contract N00014-75-C-0822, April, 1976.

2. Baum, Dennis W. et al, "Research on Nonideal Plasmas," Artec Associates Incorporated, Final Report 126, Navy Contract NR099-414/05-05-77 (473), May, 1978.

3. Baum, Dennis W., Gill, Stephen P., Shimmin, W. Lee, Mukherjee, D., Flagg, Robert F. and Watson, John D., "Shock Physics of Nonideal Plasmas," Artec Associates Incorporated, Annual Report 130, Navy Contract N00014-78-C-0354, April, 1979.

4. Rogov, V. S., "Calculation of Plasma Conductivity," Tepl. Vys. Temp., 8, 1970, p. 689.

5. Mukherjee, D., "Nonideal Effects in Dense Argon and Xenon Plasmas," Proceedings of First ONR Nonideal Plasma Workshop, Pasadena, California, 14-15 November, 1978.

6. Rogers, F. J., Ross, M., Haggin, G. L. and Wong, L. K., "Equations of State for Self-Excited MHD Generator Studies," Lawrence Livermore Laboratory, UCID-18557, February, 1980.

7. Watson, J. D. and Baum, D. W., "High Velocity Projectile/Warhead Experiments," Artec Associates Incorporated, Final Report 127, BMD Contract DASG60-78-C-0026, June, 1980.

8. Brown, P. S. and Lohmann, M. L., "Computer Modeling of the Voitenko Shock Tube Generator," Lawrence Livermore Laboratory, UCRL-81701, March, 1979.

9. Baum, Dennis W. et al, "Development of High Energy Density Simulator," Artec Associates Incorporated, Final Report 120, Defense Nuclear Agency Contract DNA001-75-C-0271, December, 1976.

10. Hoffman, R., "Stealth - A Lagrange Explicit Finite-Difference Code for Solids, Structural and Thermo-hydraulic Analysis," EPRI NP-260, August, 1976.

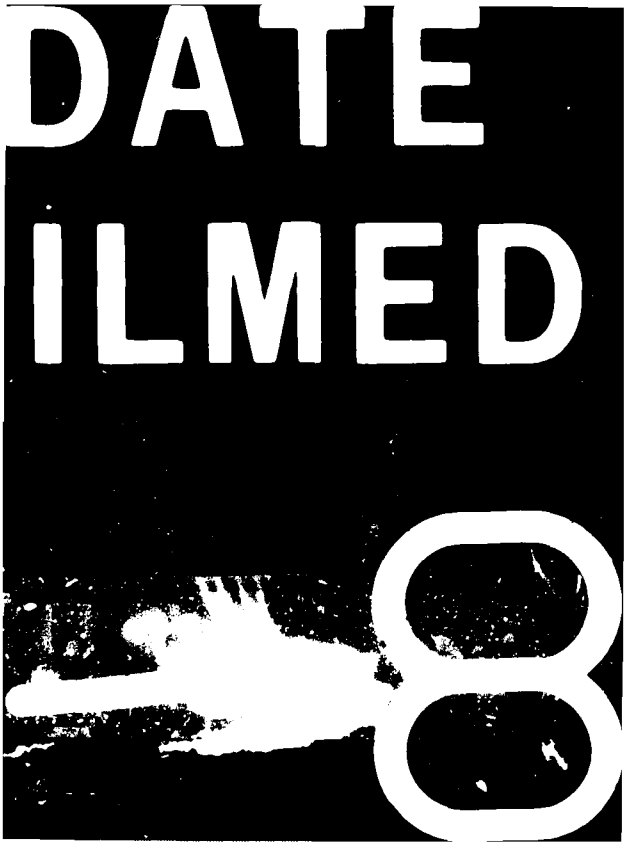
DATE
ILMED
8